frontiers | Frontiers in Earth Science

TYPE Original Research
PUBLISHED 29 August 2022
DOI 10.3389/feart.2022.984463

OPEN ACCESS

EDITED BY
Shuai Yin,
Xi'an Shiyou University, China

REVIEWED BY
Meng Wang,
Chongqing University of Science and Technology, China
Fuhua Shang,
China University of Mining and Technology, China

*CORRESPONDENCE
Guanxiong Ren,
rgxxly1991@163.com

SPECIALTY SECTION
This article was submitted to Structural Geology and Tectonics, a section of the journal Frontiers in Earth Science

RECEIVED 02 July 2022
ACCEPTED 21 July 2022
PUBLISHED 29 August 2022

CITATION
Ren G, Qin Q, Qin Z, Guo Y and Ye Z (2022), Effects of diagenesis on quality of deep dolomite reservoirs: A case study of the Upper Cambrian Xixiangchi Formation in the eastern Sichuan Basin, China.
Front. Earth Sci. 10:984463.
doi: 10.3389/feart.2022.984463

Effects of diagenesis on quality of deep dolomite reservoirs: A case study of the Upper Cambrian Xixiangchi Formation in the eastern Sichuan Basin, China

Guanxiong Ren[1,2]*, Qirong Qin[1,2], Zhangjin Qin[3], Yanbo Guo[4] and Zhaoyang Ye[4]

[1]School of Geosciences and Technology, Southwest Petroleum University, Chengdu, China, [2]State Key Laboratory of Oil and Gas Reservoirs Geology and Development Engineering, Southwest Petroleum University, Chengdu, China, [3]Exploration Division, Southwest Oil and Gas Field Company, Petro China, Chengdu, China, [4]Chongqing Gas Field, Southwest Oil and Gas Field Company, Petro China, Chengdu, China

With the Upper Cambrian Xixiangchi Formation in the eastern Sichuan Basin as the target, this study investigates various diagenetic events during different diagenetic stages in deep dolomite reservoirs, accompanied by evaluations of their effects on the formation and evolution of the reservoir rock. A series of experiments are implemented on core and outcrop samples, including petrologic analysis, fluid inclusion analysis, rare earth and minor element investigation, and carbon and oxygen isotope test. During the syngenetic (syndepositional and penecontemporaneous) diagenesis stage, dolomitization is closely related to evaporation concentration and seepage reflux of high-salinity seawater, which facilitates the reservoir rock development by greatly enhancing the permeability of the reservoir. Meanwhile, a small number of secondary pores are generated in the sediments subjected to episodic atmospheric exposure and thus affected by meteoric water. During the early diagenesis stage, recrystallization transforms part of the granular dolomite into the crystalline dolomite with or without the phantom of the grain texture. It also alters the original rock's pore structure and improves the effective primary porosity. Thus, recrystallization is key in forming the crystalline dolomite reservoir rock. However, compaction, cementation, and filling lead to the loss of massive early-formed primary pores and some secondary pores. During the mesodiagenesis-late diagenesis stage, the burial karstification, related to organic matter maturation, is the most direct control factor of the effective reservoirs space formation, and its alteration effect on the reservoir rock is related to the early process. This research helps to better identify the impact of various diagenetic processes during different diagenetic stages upon the formation and evolution of the deep dolomite reservoir rock, and it also

helps analyze the relationships among these diagenetic processes. The findings of this research provide valuable references for investigating the formation mechanism of the deep dolomite reservoir rock in the Sichuan Basin.

KEYWORDS

Xixiangchi formation, east sichuan basin, deep dolomite reservoir, fluid inclusion, diagenesis 5 processes

1 Introduction

With continuous technological progress and ever-increasing demand for hydrocarbon resources, deep buried carbonate reservoirs have become an important target for hydrocarbon exploration and exploitation. In particular, the deep dolomite reservoirs are an important contributor to new commercial discoveries of oil and gas (Dyman et al., 2002; Zhai et al., 2012; Jiao et al., 2015; Liu et al., 2020; Liu L. H. et al., 2017; Li et al., 2021). At present, the known deepest oil and gas reservoirs in the world are in the Jack and St. Malo field of the Lower Tertiary Trend in the U.S.Gulf of Mexico, which has a burial depth of 8,839 m, a hydrocarbon reserve of $6{,}821 \times 10^4$ t oil equivalent, and a production rate up to 818 t/d during testing (Pang, 2010; Jiao et al., 2015; He et al., 2016; Li et al., 2021c). The deepest gas reservoir in the world is the Mills Ranch Field in the Anadarko Basin of Western Oklahoma, and its target layer is the Lower Ordovician dolomite at a depth interval of 7663–8103 m, with a maximum single-well gas production rate of 6×10^4 m^3/d and the recoverable gas initially in place of 365×10^8 m^3 (Bai and Cao, 2014; Jiao et al., 2015; Liu et al., 2020; Li et al., 2021). In China, a series of great progress has been made in the exploration of deep dolomite reservoirs, including those in the Ordovician–Cambrian of the Tarim Basin, Ordovician, and Cambrian in the Ordos Basin, as well as Permian, Sinian, and Cambrian in the Sichuan Basin (Qian et al., 2007; Zou et al., 2014; He et al., 2017; Zhang et al., 2017; Fu et al., 2019; Gao 2019). However, the deep dolomite reservoirs in China are formed in a way that is greatly different from that in other countries, as they are typically more ancient, deeper buried, and of longer formation processes (He et al., 2016; Zhang et al., 2017; Ma et al., 2019; Ma X. H. et al., 2019; Li et al., 2021). Correspondingly, the reservoir rock presents extremely complicated characteristics due to the superimposition of multiple diagenetic events during the burial process (Moor and Druckman, 1981; Yang et al., 2008; Shen et al., 2015). Therefore, understanding the relationship among different diagenetic events of different diagenetic stages and the effects of these events on the formation and evolution of the deep dolomite reservoirs is vital to exploring deep dolomite reservoirs.

Multiple wells drilled into the Upper Cambrian Xixiangchi Formation in the eastern Sichuan Basin have produced industrial gas streams, demonstrating high potential for natural gas exploration (Li et al., 2016; Jia et al., 2021). Exploration practice and data show that the reservoir rock in the Upper Cambrian Xixiangchi Formation in the eastern Sichuan Basin has the following features: First, the reservoir rock is highly heterogenous; second, the reservoir rock develops in the layered dolomite; third, the reservoir rock occurs not only in the frequently-seen granular dolomite but also in the crystalline dolomite; fourth, the reservoirs space is mostly attributed to secondary dissolution pores, with seldom primary pores. These features all imply the impacts of diagenesis upon the reservoir rock. Nonetheless, previous studies on diagenesis only focus on dolomitization and karstification, and they generally ignore the influences of other diagenetic processes on the reservoir rock and the relationship among different diagenetic processes. Moreover, it remains controversial when it comes to dolomitization and karstification.

This paper targets the Upper Cambrian Xixiangchi Formation in the eastern Sichuan Basin and performs analyses on drilling core samples and field outcrops, such as fluid inclusion, and geochemical tests.

(1) Reconstruct the diagenetic history of the deep dolomite reservoirs of the Xixiangchi Formation;
(2) Identify the specific diagenetic process and the corresponding diagenetic stage at which it occurs;
(3) Discuss the effects of various diagenetic processes on the formation and evolution of the deep dolomite reservoirs in the Xixiangchi Formation, and explore the relationships among these diagenetic processes.

2 Geological setting

The study area is located in the eastern Sichuan Basin of Southwest China Figure 1A. The Sichuan Basin lies on the relatively northwestern side of the Yangtze platform and is surrounded by the Daba and Micang Mountains in the north, the Longmen Mountain in the west, the Lou and Daliang Mountains in the south, and the Qiyue Mountain in the east (Zou et al., 2014; Wei et al., 2018; Jin et al., 2020). It is a subordinate structural unit of the Yangtze platform. The basin and basement are formed during the Yangtzeian, Caledonian, Hercynian, Indosinian, Yanshanian, and Himalayan (Deng, 1992; He et al., 2011; Li et al., 2011). The early basin is formed during the Indosinian stage, then affected by multi-

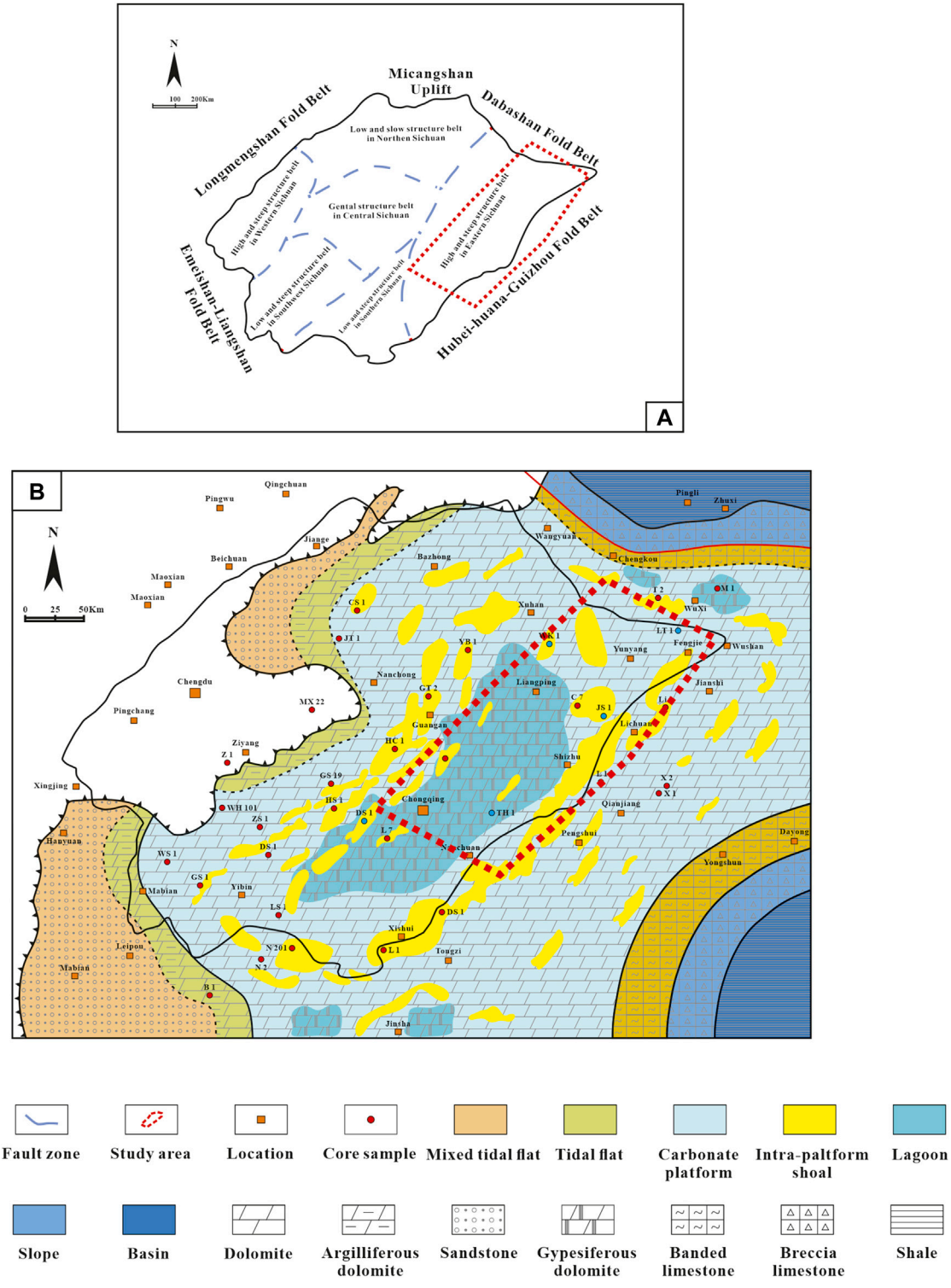

FIGURE 1
Geological survey of the study area. **(A)** Simplified map of the Sichuan Basin showing six subordinate structural belts. **(B)** The paleogeographic map of the Sichuan Basin and its adjacent areas during the Xixiangchi Formation (Modified from Li et al., 2016). The marked blue wells are sampling wells.

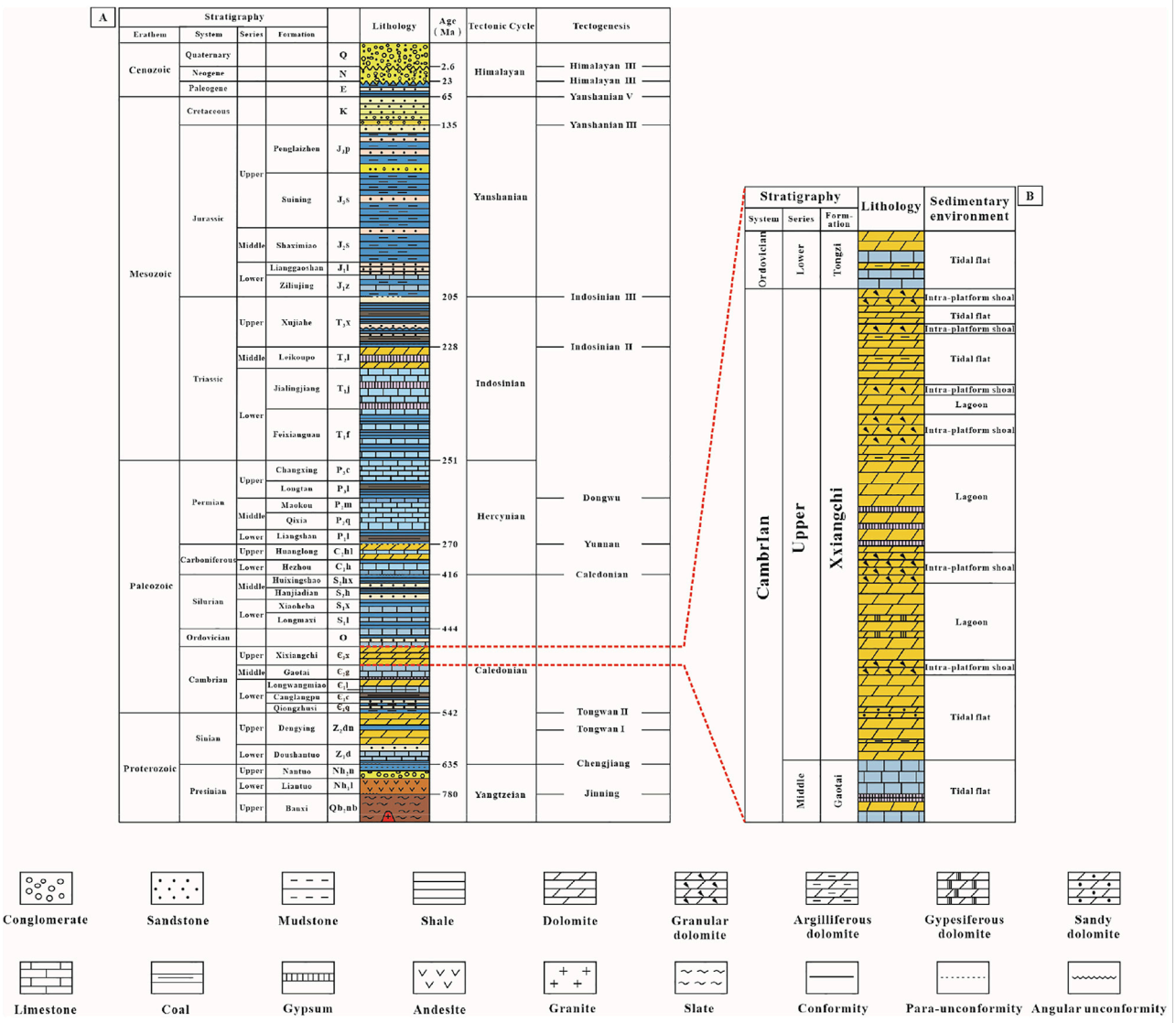

FIGURE 2
Comprehensive histogram of strata in the study area. **(A)**. Composite columnar section of the Presinian-Quaternary system of Sichuan Basin (Modified from Wei et al., 2018). **(B)**. Comprehensive stratigraphy of Xixiangchi Formation.

stage tectonic movement such as the Himalayan folding movement, and finally evolves into the current large multi-cycle-superimposed rhombic structural basin (Wang and Jin, 2002; Liu et al., 2011; Li et al., 2019). According to the regional tectonic characteristics, current tectonic features, and previous studies, the Sichuan basin is divided, by two major fault systems, namely the Huangyingshan and Longquanshan fault systems, into three structural zones, which are composed of six subordinate structural belts, namely high and steep structure belt in the Eastern Sichuan, Low and steep structure in Southern Sichuan, Low and steep structure belt in Southwest Sichuan, High and steep structure belt in Western Sichuan, Low and slow structure belt in Northern Sichuan, and Gental structure belt in Central Sichuan (Zhou et al., 2016; Li et al., 2019; Li H. K. et al., 2019, 2020, Li et al., 2021; Jia et al., 2021) Figure 1A. The study area lies within high and steep structure belt in the Eastern Sichuan.

As the top lithostratigraphic unit of the Cambrian in the Sichuan Basin, the Xixiangchi Formation continuously overlies the Middle Cambrian Gaotai Formation and underlies the Lower Ordovician Tongzi Formation (Figure 2A). During the Xixiangchi Period, the Sichuan Basin presents itself as a relatively stable cratonic deposition area, which almost completely inherits the paleogeographic pattern of the early and middle Cambrian, except for the further expansion of the Kangtien, Motianling, and Hannan ancient lands that are closely

adjacent to the western part of the basin (Feng et al., 2002; Zhang et al., 2010; Jia et al., 2021; Fan et al., 2022; Li et al., 2022).

The ancient land can provide terrigenous clasts, which results in the mixed tidal flat deposition dominated by fine-grained carbonate and clastic rocks. The middle and eastern parts of the basin are far from the ancient lands and thus mainly present the sedimentary formation of the carbonate platform facies. The Central Sichuan area, affected by the Leshan-Longnvsi paleo-uplift, is found with relatively thin deposition and shallow water depth. It mainly develops the tidal flat and intra-platform shoal deposits, mostly consisting of dolarenite, dolomicrite, and silty crystalline dolomite (Liu et al., 2017; Shi et al., 2020; Li et al., 2021c) Figure 1B. The deposition water depth of the study area is deeper than that of the Central Sichuan, and yet they share similar sedimentary environments. However, it should be noted that the restricted lagoon deposition, featuring interbedding of dolomicrite and silty crystalline dolomite, and gypsum-salt rock or gypsum salt-bearing dolomite, occurs around the intra-platform shoal deposition (Li et al., 2016; Shi et al., 2020) (Figure 2B).

3 Materials and methods

A total of 166 samples were obtained from 5 wells and 3 outcrop profiles in the Xixiangchi Formation in this study. To ensure the reliability of this study, samples should be collected and selected in accordance with the following principles:1) samples shall not be collected from the development parts such as structurally crushed and weathered zones; 2) fresh debris samples shall be selected. 3) Samples with obvious terrigenous matters and clay minerals shall be excluded.

210 thin sections were prepared for the study on petromineralogy and diagenesis. And petrologic observation and studied using the DM2500P Leica optical microscope. A thick double-face-polished thin section was prepared with 30 representative samples. On this basis, the homogenization temperatures (Th) of the fluid inclusions were tested using a Leica polarized light microscope carrying a THMSG600 geological cold-hot bench with the temperature measurement ranging from -196 to 600°C with a temperature accuracy of 0.2°C.

Geochemistry was analyzed based on the study of petrology. Besides, calcite veins and sparry calcite cements should be screened after a careful selection was performed on the sample for geochemical analysis to ensure the selected sample's reliability better. The sample was slowly ground to 74 μm in an agate mortar and was quartered. By retaining one for backup, the other three samples were applied for analyzing minor elements, carbon and oxygen isotopes, and rare earth elements. Orthophosphoric acid was adopted in the analytical test of carbon and oxygen isotopes. Specifically, powder samples are dissolved by phosphoric acid at 90°C to release carbon dioxide (CO_2). The generated CO_2 is converted into the MAT252 stable isotope mass spectrometer (Thermo Finnigan) via capillary tubes for analysis. The acquired data are converted to the PDB scale using the reference material NBS 19, and the standard deviations of $\delta^{13}C$ and $\delta^{18}O$ are 0.04 and 0.07%, respectively. The trace and rare earth elements are measured via the *in-situ* LA-ICP-MS analysis using the Agilent 7,700 Series Quadrupole ICP-MS (Agilent Technologies, United States) and the GeoLasPro 193 nm Excimer Laser Ablation System (Coherent, United States). The laser beam diameter is 25 μm, with a frequency of 8 Hz and an energy density of 10.61 J cm^{-2}, and the carrier gas is helium. The synthetic silicate glass of NIST SRM 610 is used as the external reference, while calcium (^{43}Ca) is used as the internal reference. Measurement of trace and rare earth elements is performed at Southwest Petroleum University.

4 Results

4.1 Petromineralogy

According to dolomite morphology, crystal size, and contact relation between minerals, the dolomite in the Xixiangchi Formation of the study area is mainly divided into three types: matrix, cement, and filling dolomite (MD, CD, and FD).

Matrix dolomite (MD) in the study area is divided into two types according to the preservation degree of the original rock texture (Zenger et al., 1980; Fang et al., 2003). One is the dolomite with the original rock texture, mainly including dolomicrite (MD 1) and granular dolomite (MD 2). The other is the crystalline dolomite (MD 3-1, MD 3-2, MD 3-3, and MD 3–4) with unidentifiable original rock texture.

Dolomicrite (MD 1) has extremely tiny crystallines, typically smaller than 0.005 mm, and thus it preserves a more original rock texture. The dolomite of this type is mainly subhedral–anhedral, with mosaic contact among crystallines. This type of dolomite is often seen with interbedding with gypsum-salt rock or an interlayer occurrence with gypsum-salt rock. Under the microscope, microalgae laminated texture and development of moldic pores in gypsum salt minerals are observed (Figure 3A), indicating that such dolomite is the product of early dolomitization under the arid climate.

Granular dolomite (MD 2) is the main reservoir rock type in the study area, with dominant sand-sized grains (Figure 3B), followed by oolith-sized and gravel-sized ones. The algal binding phenomenon is occasionally observed. The grain content reaches 60–80%. The gravel-sized grains typically have 2–15 mm diameters, while the others have diameters of 0.16–0.4 mm. Most grains have relatively regular shapes, typically sub-rounded to rounded, except for the sand-sized algae particles that are irregular in shape. Dolomitic cement is frequently observed among grains.

Crystalline dolomite (MD 3) in the study area can be divided into silty, fine, medium, and hetero-crystal crystalline dolomite

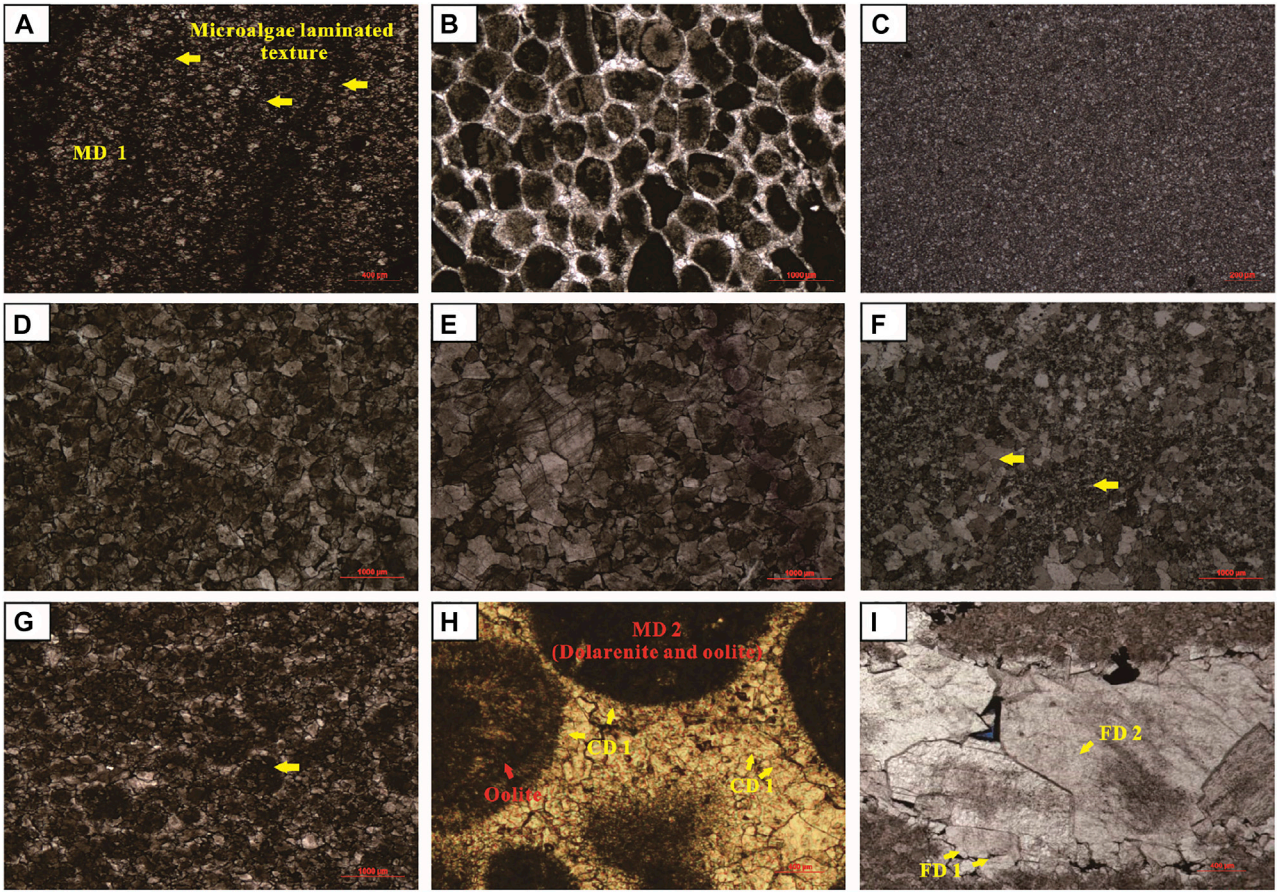

FIGURE 3
Petrographic characteristics of reservoirs. **(A)** A thin section micrograph shows the dolomicrite (MD 1) with microalgae laminated texture. **(B)** Micrograph of the thin section shows the granular (oolite) dolomite (MD 2). **(C)** Micrograph of the thin section shows the silty crystal dolomite (MD 3-1). **(D)** Micrograph of the thin section shows the fine crystal dolomite (MD 3-2) **(E)** Micrograph of the thin section shows the medium crystal dolomite (MD 3-3). **(F)** Micrograph of the thin section shows the hetero-crystal crystalline dolomite (MD 3–4). **(G)** Micrograph of the thin section shows the crystalline dolomite with the phantom of the grain texture. **(H)** The cement dolomite of the first stage (CD 1) and the dolomite cement of the second stage (CD 2). **(I)** The filling dolomite of the first stage (FD 1) and The filling dolomite of the second stage (FD 2).

(MD 3-1, MD 3-2, MD 3-3, and MD 3–4), according to the crystal sizes.

Silty crystalline dolomite (MD 3-1) is composed of tiny (0.03–0.05 mm) subhedral and euhedral crystals, with occasionally seen turbid core and bright rims (Figure 3C). Grains are tightly packed with mosaic contact among each other, and dissolution, and inter crystal pores well develop.

Fine crystalline dolomite (MD 3-2) has crystal diameters typically of 0.05–0.25 mm, with various (i.e., anhedral, subhedral, and euhedral) crystalline forms (Figure 3D). The subhedral–euhedral fine crystalline dolomite is abundant, with occasionally seen turbid core and bright rims accompanied by well-developed pores that are semi-filled to filled by bitumen. The less abundant anhedral–subhedral fine crystalline dolomite is associated with the dirty crystals surface, concave-convex contact among crystals, and limited development of pores.

Medium (MD 3-3) (Figure 3E)and hetero-crystal crystalline dolomite(MD 3-4) (Figure 3F) are mostly composed of anhedral–subhedral dolomite crystals with tight mosaic contact. In such dolomite, pores seldom develop, and thus the reservoir's capacity is low. In addition, the microscopy shows that some crystalline dolomite presents the granular phantom texture (Figure 3G) and is observed with the development of cross-bedding in the field outcrop, which suggests that part of the fine crystalline dolomite is attributed to the high-energy grain shoal deposition, and yet has its texture altered during diagenesis.

Fibrous cement dolomite (CD 1) presents itself as a circular belt with uniform thickness around the intergranular pores or the edge of grains (Figure 3H). The fibrous crystalline form is generally formed in a seawater environment. In most cases, aragonite and high-magnesium calcite are the initial carbonate sediments in seawater. The aragonite is mostly fibrous and

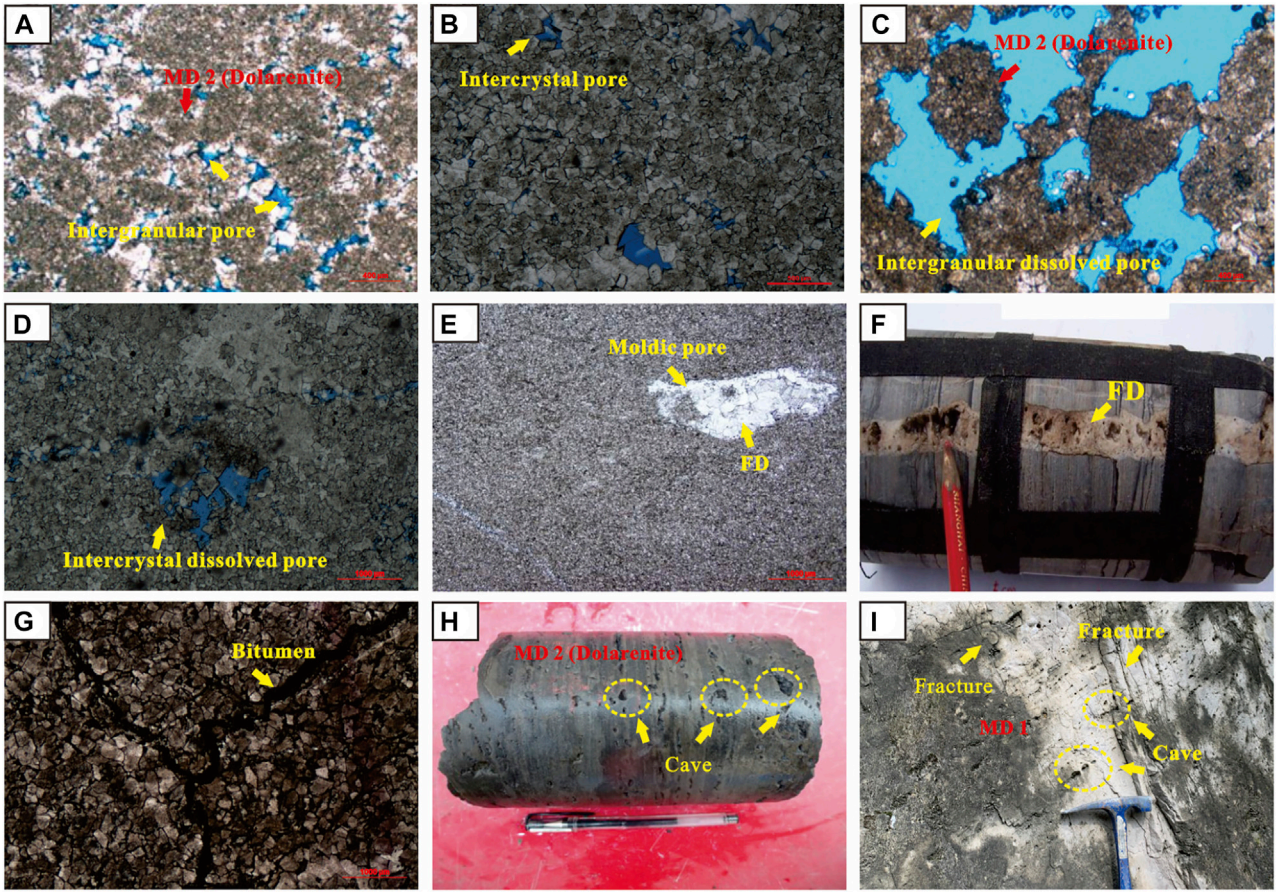

FIGURE 4
The reservoirs space type of Xixiangchi Formation. **(A)** Intergranular pores, granular (dolarenite)dolomite (MD 2).**(B)** Intercrystal pores **(C)** Intergranular dissolved pores. **(D)** Intercrystal dissolved pores, silty dolomite (MD 3-2) with dissolved crystals edge. **(E)** Moldic pores filled by dolomite. **(F)** Fractures are expanded by dissolution. **(G)** Fractures filled by bitumen. **(H)** Caves attributed to dissolution expansion of the residual intergranular pore in the granular dolomite. **(I)** Caves formed during the dissolution and alteration of the gypsum-salt moldic pore of the crystalline dolomite.

needle-like, while the high-magnesium calcite is the fiber with the uniform thickness or leaf-like crystals (Zenger et al., 1980; Fang et al., 2003; Zhang et al., 2014b). Hence, fibrous cement dolomite (CD 1) should be formed in a seabed diagenetic environment.

Granular cement dolomite (CD 2) is mostly anhedral crystals forms and tight mosaic contact among crystals (Figure 3H). Such cement generally occurs along the periphery of fibrous cement dolomite, and some are found with direct contact with grains.

Filling dolomite of the first stage (FD 1) normally occurs close to the secondary pores as well as caves and edges of fractures (Figure 3I). The dolomite crystals are mostly fine and medium-sized, with dominant subhedral and euhedral crystals forms and flat crystals surfaces.

Filling dolomite of the second stage (FD 2) presents crystals larger than those of the first stage-filling dolomite (FD 1), mostly medium and coarse sized, with some macro crystals (Figure 3I). The second stage-filling dolomite (FD 2) often develops above the first stage-filling dolomite (FD 1) and presents conformity or unconformity contact with the first stage-filling dolomite.

4.2 Types of reservoir space

According to its genesis, morphology, dimension, and distribution position, the reservoir space of the Xixiangchi Formation in the study area is divided into three types, namely pores, karst caves, and fractures. The pores include intergranular pores, inter crystal pores, intergranular dissolved pores, inter crystal dissolved pores, and moldic pores.

Intercrystal pores with regular shapes mainly occur in the dolomicrite (MD 1) and crystalline dolomite (MD 3) with relatively high euhedral degrees (Figure 4B). The size of the crystals controls the pore dimension. Intergranular pores primarily develop in the granular dolomite (MD 2), residual intergranular pores after multi-stage cementation and filling

TABLE 1 Na_2O, K_2O,BaO,FeO, MnO and FeO/MnO values of filling dolomite (FD) and cement dolomite (CD) in Xixiangchi Fm.

Sample	Lithology	Na_2O (ppm	K_2O (ppm)	BaO (ppm)	FeO (ppm)	MnO (ppm)	FeO/ MnO	Sample	Lithology	Na_2O (ppm)	K_2O (ppm)	BaO (ppm)	FeO (ppm)	MnO (ppm)	FeO/ MnO
JS-2-1	FD 1	12.82	20.18	333.06	328.69	1000.06	0.33	WK-3-1	CD 1	543.20	333.87	1123.84	798.44	837.79	0.95
JS-2-4	CD 1	512.85	435.28	927.36	445.28	464.08	0.96	WK-4-1	CD 1	555.28	367.82	1282.19	803.33	785.68	1.02
JS-4-1	CD 2	158.23	218.22	815.97	549.61	1125.08	0.49	DS-2-1	CD 2	181.62	141.22	743.65	156.36	572.99	0.27
JS-4-2	CD 2	145.22	194.59	1089.34	92.24	400.39	0.23	DS-2-2	CD 2	245.57	148.57	482.00	911.28	1008.38	0.90
JS-8-1	CD 1	684.72	281.23	3821.55	557.52	513.22	1.09	DS-3-1	CD 1	642.85	301.55	1063.85	925.09	1015.38	0.91
JS-8-2	FD 1	15.10	28.13	223.54	302.27	789.01	0.38	DS-4-4	FD 1	28.56	15.28	416.55	167.34	203.51	0.82
JS-8-3	FD 2	173.22	355.11	1238.38	133.02	1325.80	0.10	JFS-3	FD 2	65.81	128.30	894.33	278.25	1752.38	0.16
TH-1-2	CD 2	91.48	152.32	882.37	647.28	857.83	0.75	JFS-17	CD 1	700.55	318.46	2594.36	332.62	358.74	0.93
TH-1-3	FD 1	54.28	40.74	608.09	286.34	555.00	0.52	JFS-22	CD 2	108.38	200.48	545.81	468.75	763.44	0.61
TH-6-1	FD 1	44.67	37.35	141.23	105.49	294.73	0.36	JFS-27	FD 1	61.23	41.92	987.27	358.41	1334.56	0.27
TH-6-2	FD 2	158.94	380.54	91.28	48.44	854.27	0.06	JFS-28	FD 2	108.46	184.72	809.43	31.46	996.66	0.03
TH-6-5	FD 1	41.28	35.86	535.72	131.51	115.89	1.13	JSP-1	FD 2	25.66	99.17	448.56	202.67	2019.99	0.10
LT-5-1	FD 2	161.57	275.49	1526.73	58.49	154.26	0.38	JSP-8	CD 1	615.80	298.45	1845.88	765.81	801.66	0.96
LT-5-2	CD 2	204.29	172.28	687.51	644.00	825.77	0.78	JSP-9	CD 1	662.74	401.20	872.59	310.06	399.53	0.78
LT-7-6	CD 1	502.23	424.26	3044.18	923.82	1007.12	0.92	JSP-13	CD 2	213.77	163.85	1210.14	666.66	929.18	0.72
LT-10-3	FD 1	37.29	28.37	770.00	412.25	774.87	0.53	NC-1	CD 1	718.22	385.23	825.37	512.26	497.81	1.03
LT-10-4	FD 2	38.29	111.67	112.90	220.59	2282.18	0.10	NC-12	FD 2	188.14	378.24	1111.44	188.37	478.64	0.39
WK-1-1	FD 2	139.22	48.83	610.05	199.57	1932.21	0.10	NC-13	CD 2	151.84	130.71	777.29	428.03	388.59	1.10
WK-2-1	FD 1	48.34	34.19	567.64	88.47	165.26	0.54	NC-27	FD 1	57.89	38.62	1754.01	399.00	518.75	0.77
WK-2-2	CD 2	281.73	238.56	421.11	831.01	1350.24	0.62	NC-28	FD 2	99.38	185.31	708.28	250.04	1777.48	0.14

10.3389/feart.2022.984463

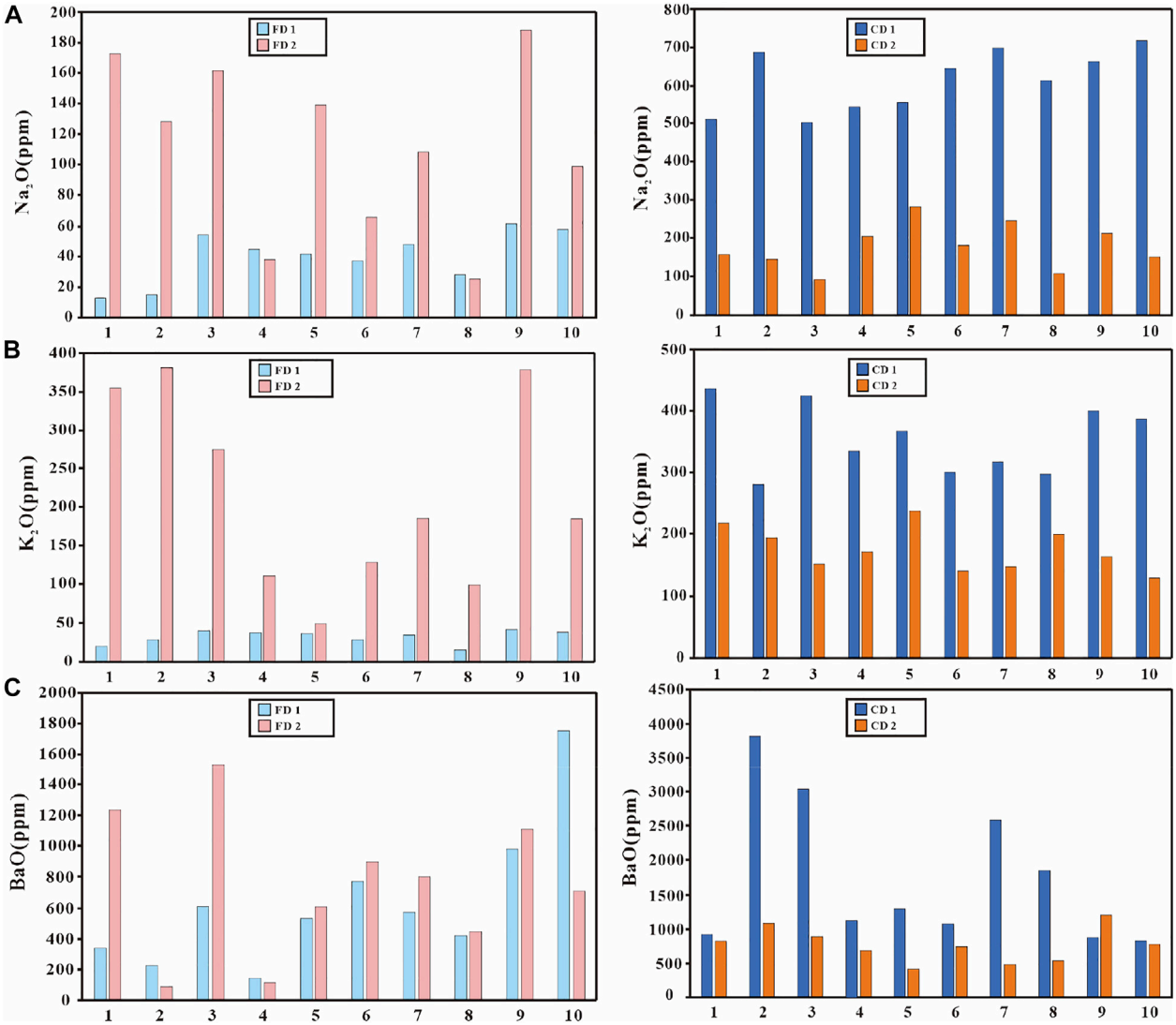

FIGURE 5
Histogram showing the variation of Na_2O, K_2O, and BaO contents of filling dolomite (FD) and cement dolomite (CD). **(A)** Variation in the Na_2O concentrations of the FD and CD. **(B)** Variation in the K_2O concentrations of the FD and CD. **(C)** Take in the BaO concentrations of the FD and CD.

among grains, and some framework pores among alga bindstones (Figure 4A). These pores are mostly oval and irregular. Intercrystal dissolved pores are most developed in the crystalline dolomite (MD 3) of the Xixiangchi Formation in the study area (Figure 4D). They derive from the expansion of inter crystal pores induced by dissolution. Intergranular dissolved pores are the main contributor to the reservoirs space of the granular dolomite in the Xixiangchi Formation of the study area (Figure 4C). The boundaries of the pores are smooth and, in most cases, harbor-like. Some pores are observed with undissolved residual cement. In the case of intensive dissolution, the residual sparry cement is unseen, and relatively large pores are formed. Moldic pores are often observed in the dolomicrit and silty crystalline dolomite that contains anhydrite nodules or rock salts (Figure 4E). The anhydrite nodule and rock salt are dissolved during the meteoric diagenetic environment, and the gypsum and salt moldic pores occur, which are mostly filled later by dolomite and bitumen.

Petrographic observations indicate that there are at least two stages of fractures. These fractures are mostly horizontal and high-angle ones, characterized by short extension, narrow opening, and filling or semi-filling of bitumen (Figure 4G). Nevertheless, some fractures are found with long extension, irregular fracture edges, and extremely coarse fracture surfaces, representing dissolution's effect. The structural suture

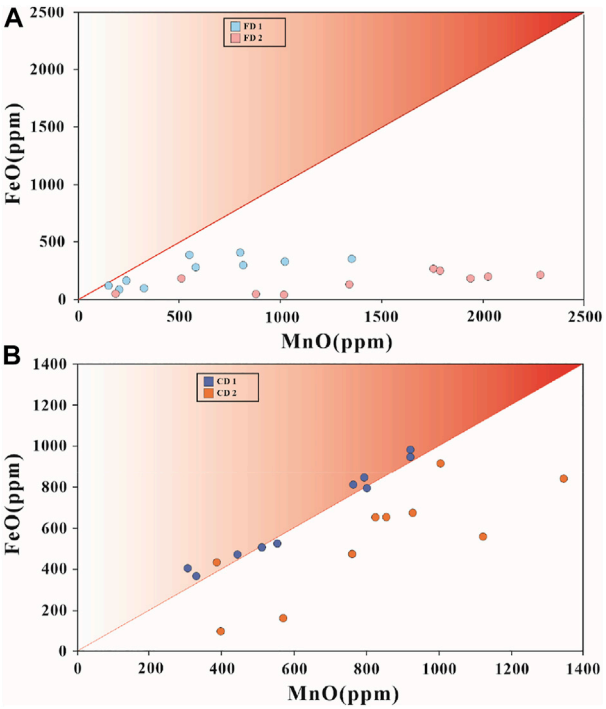

FIGURE 6
Relationship between FeO and MnO values of filling dolomite. **(A)**. FD1, **(B)**. FD2.

line is often high-angle or zigzagged and typically cuts the early structural fracture, which is considered the product of pressure solution along the vertical stress direction (Jiang et al., 2015; Liu et al., 2020).

The cave refers to pores with diameters larger than 2 mm. In other words, karst caves are formed due to the further expansion of various dissolved pores (Zhu et al., 2015; Li, 2002). Two types of karst caves occur in the Xixiangchi Formation of the study area. The first type is attributed to dissolution expansion of the residual intergranular pore in the granular dolomite, which, together with the intergranular pore, constituents good reservoirs space (Figure 4H). The other type is formed during the dissolution and alteration of the gypsum-salt moldic pore of the crystalline dolomite, which is often partially filled by bitumen and dolomite minerals. Such karst caves are found with limited contributions to reservoirs (Figure 4I).

4.3 Geochemistry

4.3.1 Minor elements

The minor element measurements of cement dolomite and filling dolomite (CD and FD) are summarized in Table 1. For the cement dolomite, the Na_2O content is 91.48–718.22 ppm; K_2O, 130.71–435.28 ppm; BaO, 421.11–3,821.55 ppm; FeO, 92.24–925.09 ppm; MnO, 358.74–1,350.24 ppm (Figures 5A–C). What's noteworthy is that the Na_2O, K_2O, and BaO contents of fibrous cement dolomite (CD 1) are higher than those of granular cement dolomite (CD 2). In addition, the FeO/MnO ratio of fibrous cement dolomite (approximately equal to about one) is higher than those of granular cement dolomite (obviously below one) (Figure 6B).

For the filling dolomite, the Na_2O content is 12.82–188.14 ppm; K_2O, 15.23–380.54 ppm; BaO, 91.28–1754.01 ppm; FeO, 31.46–412.25 ppm; MnO, 115.89–2282.18 ppm (Figures 5A–C). The Na_2O, K_2O, and BaO contents of the first stage-filling dolomite (FD 1) are relatively low, and the FeO/MnO ratio is below one. Compared with the first stage-filling dolomite (FD 1), the second stage-filling dolomite (FD 2) presents even lower Na_2O, K_2O, BaO contents, and lower FeO/MnO ratio (Figure 6A).

4.3.2 Rare earth elements

The rare earth element (REE) measurements of the matrix dolomite (MD) are presented in Table 2, which have been normalized against the Post-Archean Australian Shale (PAAS). Moreover, Ce and Eu anomalies are calculated respectively via the following equations: $Eu/Eu^* = Eu_{SN}/(0.67Sm_{SN} + 0.33Tb_{SN})$ and $Ce/Ce^* = Ce_{SN}/(0.5La_{SN} + 0.5Pr_{SN})$ (Hu et al., 2010; Liu et al., 2017; Lei et al., 2016). The total REE content (ΣREE) of the granular dolomite (MD 2) is 7.29–7.78 ppm (average 7.65 ppm); that of the dolomicrite (MD 1),9.78–10.04 ppm (average 9.86 ppm); that of the crystalline dolomite (MD 3-1, MD 3-2, MD3-3 and MD 3–4), 8.02–8.91 ppm (average 8.71 ppm). These three types of matrix dolomite (MD)are all observed with positive Ce anomaly, enrichment of light rare earth elements (LREE, from La to Nd), and loss of heavy rare earth elements (HREE, from Ho to Lu) (Figure 7).

4.3.3 Stable isotope

The carbon and oxygen isotope ratios of the matrix and filling dolomite (MD and FD) are included in Table 3. The distribution of matrix dolomite $\delta^{13}C$ is ranged from −1.46 to 0.40‰, with the $\delta^{18}O$ ranging from −11.33 % to −6.31%. The $\delta^{13}C$ values of hetero-crystal crystalline dolomite (MD 3-4) and dolomicrite (MD 1) are more negative than that of other matrix dolomites and other matrix dolomites share similar $\delta^{13}C$ values. $\delta^{18}O$ values of various matrix dolomite gradually become negative with the increase of crystal size. Besides, compared with the $\delta^{18}O$ of the seawater of the same period (during the Late Cambrian, the seawater presents $\delta^{18}O$ from -10‰ to -7%) (Veizer et al., 1999; Prokoph et al., 2008), most filling dolomite as well as fine, medium, and hetero-crystal crystalline dolomite (MD 3-2, MD3-3 and MD 3-4) have lower $\delta^{18}O$ values (Figure 8B).

$\delta^{13}C$ and $\delta^{18}O$ values of filling dolomite (FD) are ranged from −1.35% to −0.64% and from −10.98% to −8.77%, respectively. The $\delta^{13}C$ of the filling dolomite is more negative than that of the matrix dolomite. Also, the $\delta^{13}C$ and $\delta^{18}O$ values of varying filling dolomite are varied. The $\delta^{13}C$ and $\delta^{18}O$ values of filling dolomite of the second stage (FD 2) are more negative in

TABLE 2 Rare element data of the matrix dolomite (MD).

Sample	Lithology	La	Ce	Pr	Nd	Sm	Eu	Gd	Tb	Dy	Ho	Er	Tm	Yb	Lu	∑Ree	δCe	δEu	L/H
JS-2-1	MD 1	0.48	3.87	0.82	0.68	0.71	0.56	0.50	0.41	0.36	0.31	0.28	0.28	0.26	0.28	9.80	5.95	0.93	2.66
JS-4-2	MD 2	0.31	3.52	0.61	0.52	0.50	0.37	0.35	0.28	0.23	0.15	0.09	0.12	0.11	0.13	7.29	7.65	0.87	3.99
JS-7-3	MD 3-1	0.38	3.75	0.66	0.56	0.59	0.48	0.43	0.40	0.35	0.31	0.27	0.26	0.23	0.20	8.87	7.21	0.94	2.62
JS-7-4	MD 3-3	0.42	3.58	0.62	0.52	0.49	0.40	0.37	0.33	0.29	0.26	0.22	0.18	0.19	0.15	8.02	6.88	0.93	3.03
TH-1-4	MD 3-3	0.33	3.64	0.56	0.54	0.58	0.52	0.48	0.42	0.38	0.36	0.28	0.25	0.21	0.17	8.72	8.18	0.98	2.42
TH-1-5	MD 3-4	0.39	3.49	0.62	0.62	0.60	0.54	0.56	0.46	0.40	0.35	0.30	0.23	0.20	0.15	8.91	6.91	0.93	2.36
TH-6-5	MD 2	0.34	3.69	0.58	0.50	0.54	0.40	0.43	0.33	0.29	0.20	0.08	0.10	0.10	0.15	7.73	8.02	0.82	3.60
LT-5-1	MD 1	0.42	4.22	0.71	0.72	0.64	0.62	0.43	0.46	0.37	0.32	0.31	0.25	0.28	0.29	10.04	7.47	1.16	2.70
LT-5-2	MD 1	0.43	3.99	0.70	0.67	0.68	0.54	0.50	0.48	0.44	0.37	0.31	0.28	0.24	0.20	9.83	7.06	0.92	2.49
LT-7-6	MD 3-1	0.30	3.35	0.68	0.64	0.66	0.57	0.51	0.48	0.42	0.35	0.29	0.21	0.16	0.18	8.80	6.84	0.97	2.38
LT-10-1	MD 3-4	0.35	3.99	0.58	0.61	0.53	0.44	0.41	0.34	0.34	0.30	0.25	0.19	0.17	0.13	8.63	8.58	0.94	3.05
LT-11-5	MD 2	0.37	3.58	0.60	0.51	0.59	0.44	0.40	0.35	0.26	0.18	0.14	0.10	0.14	0.11	7.77	7.38	0.89	3.63
LT-11-6	MD 2	0.22	3.01	0.55	0.58	0.69	0.64	0.63	0.47	0.27	0.15	0.10	0.13	0.10	0.08	7.62	7.82	0.97	2.95
WK-1-1	MD 1	0.45	4.11	0.73	0.68	0.60	0.51	0.48	0.44	0.38	0.33	0.29	0.27	0.27	0.24	9.78	6.97	0.94	2.62
WK-4-2	MD 3-2	0.40	3.57	0.66	0.68	0.62	0.56	0.57	0.50	0.43	0.37	0.30	0.22	0.19	0.14	9.21	6.74	0.94	2.39
JSP-1	MD 2	0.33	3.37	0.56	0.50	0.72	0.52	0.44	0.38	0.25	0.18	0.15	0.09	0.13	0.10	7.72	7.57	0.90	3.49
JSP-8	MD 2	0.17	2.96	0.60	0.63	0.74	0.65	0.59	0.39	0.27	0.20	0.20	0.18	0.14	0.06	7.78	7.69	0.98	2.83
JSP-9	MD 3-2	0.37	4.01	0.61	0.58	0.55	0.42	0.35	0.31	0.31	0.29	0.24	0.18	0.15	0.11	8.48	8.18	0.93	3.37

[a]The data of Post-Archean Average Shale (PAAS) in normalized calculation were from Mclennan (1989). Eu and Ce, anomaly values were calculated by $Eu/Eu^* = Eu_{SN}/(0.67Sm_{SN} + 0.33Tb_{SN})$,$Ce/Ce^* = Ce_{SN}/(0.5La_{SN} + 0.5Pr_{SN})$ (Liu et al., 2017; Lei et al., 2016).

comparison to the filling dolomite of the first stage (FD 1) (Figure 8).

4.3.4 Fluid inclusions

This research finds gas-liquid two-phase fluid inclusions only in the filling dolomite (FD). The determined homogenization temperature of the fluid inclusion in the filling dolomite (FD) ranges from 70.8 to 178.6°C (Table 4). Specifically, the homogenization temperature of the fluid inclusion of filling dolomite of the first stage (FD 1) is 70.8–129.7°C, while that of the fluid inclusion of filling dolomite of the second stage (FD 2) is within 132.2–178.6°C (Figure 9).

5 Discussion

5.1 Destructive diagenesis and its impact on reservoir formation

The destructive diagenesis, unfavorable to reservoir rock development, is the main reason for the massive loss of primary pores and reduction of secondary pores. It includes compaction, pressure solution, cementation, and filling.

The Xixiangchi Formation in the study area is deeply buried and thus subjected to intensive compaction and pressure solution during its burial process (Zhao et al., 2012; Jiao et al., 2015; Li et al., 2022). However, due to the early formation of dolomite and cement in the study area, the corresponding detailed statement is presented below), these early-formed cement and grain textures of dolomite, to some extent, resist compaction. Therefore, the Xixiangchi Formation in the study area has relatively low degrees of compaction, mainly manifested as the dominance of floating contact among grains and rarely-observed grain crushing and deformation. Although the early-formed cement and dolomite, to some extent, support the framework and resist compaction, the primary porosity still declines by 20–30%.

The cement dolomite in the Xixiangchi Formation of the study area can be attributed to two stages. Fibrous cement dolomite (CD 1) was formed in a seabed diagenetic environment (Zenger et al., 1980; Fang et al., 2003). Compared with the cement of fibrous cement dolomite (CD 1), the Na_2O, K_2O, and BaO contents of the dolomite of granular cement dolomite (CD 2) are much lower, suggesting lower water salinity during this stage, possibly due to meteoric water invasion (Figures 5A–C) (Park and Schot, 1968; Lei et al., 2015; Lin et al., 2017). The FeO/MnO ratio of granular cement dolomite (CD 2) is obviously below one (Figure 6B), indicating a relatively closed diagenetic environment during the formation of such cement (Park and Schot, 1968; Lin et al., 2017). If such cement was formed in a deep burial environment, it would hardly be affected by meteoric water. Hence, it is speculated that the cement dolomite of granular cement dolomite (CD 2) should be formed in a shallow burial environment invaded by meteoric water. The cement of two-stage cementation occupies a large volume of space in the primary pores. The early-formed fibrous cement dolomite (CD 1) reduces the primary intergranular

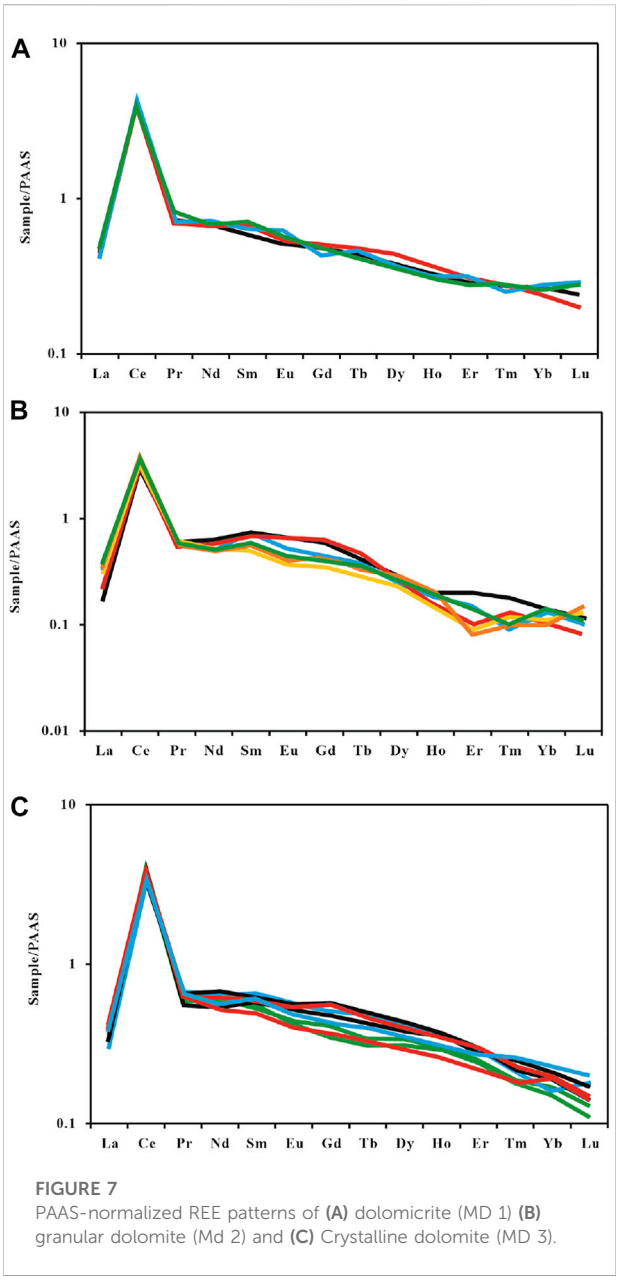

FIGURE 7
PAAS-normalized REE patterns of **(A)** dolomicrite (MD 1) **(B)** granular dolomite (Md 2) and **(C)** Crystalline dolomite (MD 3).

porosity by 5–10%, while granular cement dolomite (CD 2) with larger crystals, filling the remaining intergranular pores. Thus, the primary pores virtually completely vanish.

Dolomite also occurs in the study area's secondary pores and fractures of the Xixiangchi Formation. However, it is difficult to determine the genesis of such dolomite, and many claims that it should enter and fill the early pores and fractures in the later stage (Lin et al., 2015; Zhang et al., 2014b). Therefore, it is defined as the filling material instead of cement. There were two stages of filling in the Xixiangchi Formation. The first stage occurred in the middle-deep burial environment. The Na_2O, K_2O, and BaO contents of the first stage-filling dolomite (FD 1) are relatively low (Figures 5A–C), accompanied by the low negative $\delta^{13}C$ and the moderately negative $\delta^{18}O$ value. The FeO/MnO ratio of such filling dolomite is below one. According to the Th measurement of fluid inclusions, the burial depth should be 2000–3,500 m (Figure 9 and Figure 10). Compared with the first stage-filling dolomite (FD 1), the second stage-filling dolomite (FD 2) presents even lower $\delta^{13}C$ and $\delta^{18}O$ values (Table 3), lower Na_2O, K_2O, BaO contents (Figures 5A–C) and lower FeO/MnO ratio (Figure 6A), and considerably higher Th values of the fluid inclusions (Figure 9 and Figure 10), which suggest deeper burial depth during the formation of such filling dolomite. The second stage-filling dolomite (FD 2), should be formed in the deep burial. Besides dolomite, a small quantity of bitumen is also observed as the filling material in the Xixiangchi Formation of the study area. Filling dolomite and bitumen narrow the secondary pore and throat and reduce the reservoir rock's porosity and permeability.

5.2 Recrystallization and its impact on reservoir formation

The intensity of carbonate rock recrystallization grows with the increasing burial depth and elevated temperature (Mitchell et al., 1996; Zhao and Zheng, 2011). However, for the Xixiangchi Formation in the study area that features the same burial depth and diagenetic temperature, the difference in recrystallization intensity is mainly dependent on the composition characteristics during the deposition of the original rock. Recrystallization is suppressed in the dark dolomicrite (MD 1), dark granular dolomite (MD 2), and argilliferous dolomite that is enriched with insoluble residues such as organic and argillaceous matter because insoluble residues can effectively hinder the alteration of carbonate rock by diagenetic fluids (Veizer et al., 1999; Dyman et al., 2002; Ma et al., 2011; Qie et al., 2021). The pre- and post-crystalline structures are seen with slight differences. The dolomite crystals are still dominated by micritic crystals and are mostly anhedral–subhedral. The dolomite with uneven distribution of insoluble residues often evolves into hetero-crystal crystalline dolomite (MD 3–4) via recrystallization. The light-colored dolomicrite with only a few or no insoluble residues and other granular dolomite is found with high recrystallization intensity, which is manifested as the gradual expansion of the tiny crystal of the dolomicrite (MD 1) and destruction of the original granular texture of the granular dolomite that results in the silty and fine crystalline dolomite (MD 3-1 and MD 3-2) with or without granular phantom (Figure 11).

Recrystallization intensity can be directly revealed by the crystal size and structure of the rock, and the δ18O value can well indicate it (Li and He, 2014; Jiang et al., 2015; Li et al., 2021). With the increasing recrystallization intensity, the degree of order of crystals gradually increases, and meanwhile, the $\delta^{18}O$ value declines (Mitchell et al., 1996; Murray, 1960; Zhou et al.,

TABLE 3 δ13 C and δ18 O values of various types of dolomites in Xixiangchi Fm.

Sample	Lithology	$^{18}O_{PDB}$, ‰	$^{13}C_{PDB}$, ‰	Sample	Lithology	$\delta^{18}O_{PDB}$, ‰	$^{13}C_{PDB}$, ‰
JS-2-1	MD 1	−9.30	−0.78	WK-3-1	MD 3-1	−9.12	−0.41
JS-2-4	MD 2	−6.58	−0.40	WK-4-1	MD 3-2	−9.46	−1.28
JS-4-1	MD 1	−7.70	−0.31	WK-4-2	MD 3-2	−9.12	−0.70
JS-4-2	MD 2	−7.00	−0.62	DS-2-1	MD 3-2	−10.09	−0.42
JS-7-3	MD 3-1	−8.51	−1.21	DS-2-2	MD 3-3	−8.56	−0.90
JS-7-4	MD 3-3	−10.34	−0.89	DS-3-1	MD 3-3	−9.71	0.40
JS-8-1	MD 3-2	−10.03	−0.78	DS-4-4	FD 1	−9.43	−0.69
JS-8-2	FD 1	−9.56	−0.64	JFS-3	MD 1	−7.15	−0.72
JS-8-3	FD 2	−10.11	−0.83	JFS-14	MD 3-1	−8.61	−0.58
TH-1-2	MD 3-1	−8.31	−0.98	JFS-17	MD 3-3	−10.52	−1.13
TH-1-3	MD 3-2	−9.12	−1.46	JFS-22	MD 3-4	−10.76	−0.97
TH-1-4	MD 3-3	−10.28	−0.47	JFS-27	FD 1	−9.01	−1.33
TH-1-5	MD 3-4	−10.58	−0.61	JFS-28	FD 2	−9.67	−0.94
TH-6-1	MD 3-4	−10.23	−0.67	JSP-1	MD 2	−9.78	−1.00
TH-6-2	FD 2	−9.79	−0.92	JSP-8	MD 2	−7.22	−0.39
TH-6-5	MD 2	−9.12	−1.07	JSP-9	MD 3-2	−9.84	0.30
LT-5-1	MD 1	−8.12	−1.11	JSP-13	MD 3-3	−11.33	−0.81
LT-5-2	MD 1	−8.88	−0.74	JSP-15	MD 3-4	−11.25	−1.08
LT-7-5	MD 1	−9.64	−0.53	JSP-19	MD 3-2	−8.00	−0.70
LT-7-6	MD 3-1	−7.54	−0.53	JSP-25	MD 3-3	−9.99	−0.88
LT-7-7	MD 3-1	−9.24	−0.58	NC-1	MD 1	−6.31	−1.22
LT-10-1	MD 3-4	−10.98	−0.82	NC-12	MD 2	−7.33	−0.50
LT-10-3	FD 1	−8.77	−0.83	NC-13	MD 2	−8.01	−0.81
LT-10-4	FD 2	−10.98	−1.35	NC-18	MD 3-1	−8.37	−0.52
LT-11-3	MD 2	−6.92	−0.82	NC-19	MD 3-1	−9.92	−0.52
LT-11-4	MD 2	−8.22	−0.73	NC-20	MD 3-1	−9.03	−0.77
LT-11-5	MD 2	−8.73	−0.47	NC-23	MD 3-2	−11.02	−0.40
LT-11-6	MD 2	−7.62	−0.04	NC-24	MD 3-2	−10.87	−0.67
WK-1-1	MD 1	−8.89	−0.94	NC-27	FD 1	−9.60	−1.17
WK-2-2	MD 3-3	−10.12	−0.96	NC-28	FD 2	−9.54	−0.96

2014; Liu et al., 2018; Wang et al., 2022). This is attributed to the enhanced fractionation effect due to the improved recrystallization, which results in the loss of $\delta^{18}O$ of dolomite (Mitchell et al., 1996; Veizer et al., 1999).

During the gradual expansion of dolomite crystals, recrystallization also alters the reservoir pore, yet manifested as changes in the original pore structure instead of growth or reduction of total porosity. The inter crystal pore and crystal dissolved pore is the most developed pore types in the crystalline dolomite reservoir rock. The early-formed inter crystal pore mainly occurs in the dolomicrite (MD 1), which typically presents tiny pores and poor pore connectivity, although the pore is well developed. After recrystallization, dolomicrite (MD 1) gradually transforms into fine or silty crystalline dolomite (MD 3-1 and MD 3-2) with larger crystals, during which the early tiny intergranular pore is re-arranged and optimized. Consequently, the pore structure is altered, and the inner crystal pore with a larger storage space is formed. In addition, the euhedral degree of dolomite grows with the expansion of dolomite crystals, which tends to flatten the throats connecting pores. This, to some extent, improves the effective porosity and permeability of the reservoirs (Mitchell et al., 1996; Zhao et al., 2012) (Figure 11). To sum up, the formation of the crystalline dolomite reservoir rock is mainly attributed to recrystallization.

5.3 Dolomitization and its impact on reservoir formation

The dolomite in the Xixiangchi Formation of the study area mainly develops three types of dolo: matrixtrix, cement, and filling dolomite (MD, CD, and FD). The cement and filling dolomite (CD and FD)only occurs in the storage space, such as

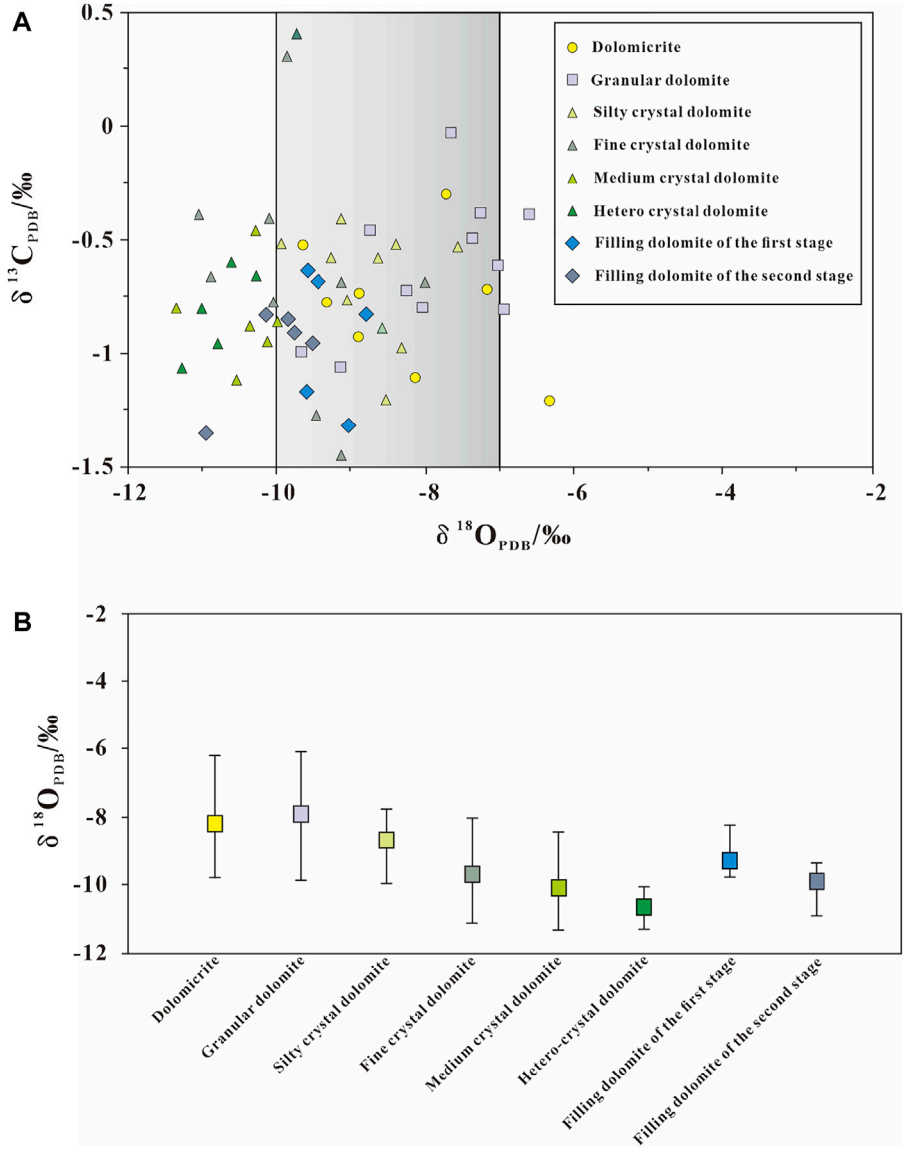

FIGURE 8
Characteristics of stable isotopes in deep dolomite reservoirs of Xixiangchi Formation in the eastern Sichuan Basin. **(A)** Cross-plot of $\delta^{13}C$ versus $\delta^{18}O$ values of various dolomite fabrics. **(B)** Variation of $\delta^{18}O$ contents of various type dolomites with the average values marked as square.

pores, karst caves, and fractures, and thus has no stratigraphic implications. Given this, the investigation of dolomitization in the study area focuses on the matrix dolomite (MD) that is stratigraphically meaningful.

The matrix dolomite (MD) in the study area has three characteristics. First, it is found with the common stratified occurrence and associated tiny crystals (dominant micritic–silty ones). Second, the vertical occurrence of dolomicrite (MD 1) is often observed as interbedding with evaporite or interlayers in evaporate. Third, the granular dolomite (MD 2), of which grains are mostly composed of dolomicrite (MD 1) and silty crystalline dolomite (MD 3-1), develops the fibrous or horse-tooth-like cement dolomite. These characteristics of the matrix dolomite (MD) eliminate the possibility of mixed-water dolomitization and highlight the possible early dolomitization closely related to evaporation concentration and seepage reflux of high-salinity seawater (Badiozamani, 1973; Li and He, 2014; Jia et al., 2021; Jia and Pang, 2015; Fan et al., 2020).

TABLE 4 Fluid inclusion data.

Sample	Lithology	TH (°C)	Sample	Lithology	TH (°C)
JS-2-1	FD 1	112.5	WK-1-1	FD 2	155.5
JS-2-1	FD 1	124.8	WK-1-1	FD 2	136.3
JS-2-1	FD 1	73.5	WK-1-1	FD 2	166.6
JS-8-2	FD 1	119.3	WK-2-1	FD 1	103.8
JS-8-2	FD 1	98.8	WK-2-1	FD 1	79.7
JS-8-2	FD 1	111.1	DS-4-4	FD 1	113.5
JS-8-2	FD 1	108.3	DS-4-4	FD 1	120.2
JS-8-3	FD 2	143.2	DS-4-4	FD 1	129.1
JS-8-3	FD 2	156.9	JFS-3	FD 2	147.3
JS-8-3	FD 2	178.6	JFS-3	FD 2	168.0
JS-8-3	FD 2	171.9	JFS-3	FD 2	173.4
TH-1-3	FD 1	77.7	JFS-3	FD 2	174.0
TH-1-3	FD 1	89.4	JFS-27	FD 1	76.1
TH-1-3	FD 1	124.6	JFS-27	FD 1	109.6
TH-1-3	FD 1	128.3	JFS-27	FD 1	122.9
TH-6-1	FD 1	82.8	JFS-28	FD 2	144.8
TH-6-1	FD 1	91.1	JFS-28	FD 2	148.0
TH-6-1	FD 1	129.7	JFS-28	FD 2	160.7
TH-6-2	FD 2	132.9	JFS-28	FD 2	175.2
TH-6-2	FD 2	136.8	JFS-27	FD 1	95.2
TH-6-2	FD 2	160.1	JFS-27	FD 1	118.7
TH-6-2	FD 2	158.6	JFS-27	FD 1	74.3
TH-6-5	FD 1	103.6	NC-27	FD 1	86.9
TH-6-5	FD 1	106.7	NC-27	FD 1	70.8
TH-6-5	FD 1	114.2	NC-27	FD 1	95.5
TH-6-5	FD 1	79.6	NC-27	FD 1	122.2
TH-6-5	FD 1	88.8	NC-27	FD 1	127.9
LT-5-1	FD 2	143.8	JS-1	FD 2	141.8
LT-5-1	FD 2	162.1	JS-1	FD 2	144.5
LT-5-1	FD 2	140.8	JS-1	FD 2	152.8
LT-5-1	FD 2	139.6	JS-1	FD 2	170.6
LT-10-3	FD 1	75.1	JS-1	FD 2	178.4
LT-10-3	FD 1	80.4	NC-12	FD 2	132.7
LT-10-3	FD 1	100.9	NC-12	FD 2	173.6
LT-10-3	FD 1	129.3	NC-12	FD 2	174.5
LT-10-4	FD 2	171.2	NC-12	FD 2	137.0
LT-10-4	FD 2	172.4	NC-28	FD 2	177.3
LT-10-4	FD 2	170.3	NC-28	FD 2	150.4
LT-10-4	FD 2	132.2	NC-28	FD 2	148.4

Besides, the geochemical evidence also proves that the matrix dolomite (MD) is not of mixed-water dolomitization. In most cases, the dolomite originating from mixed-water dolomitization presents extremely and yet greatly varied $\delta^{13}C$ values (from −10 to 20% PDB) and a narrow value range of $\delta^{18}O$(Badiozamani, 1973; Mckenzie, 1981). Clearly, the matrix dolomite (MD) in the Xixiangchi Formation of the study area shows no such characteristics concerning the $\delta^{13}C$ and $\delta^{18}O$ values. The $\delta^{18}O$ values of the fine, medium, and hetero-crystal crystalline dolomite (MD 3-2, MD 3-3, and MD 3–4) are lower than that of the contemporary seawater (during the Late Cambrian the seawater $\delta^{18}O$ ranges from -10‰ to -7%) (Veizer et al., 1999; Prokoph et al., 2008). This characteristic seems to indicate that the fine, medium and hetero-crystal

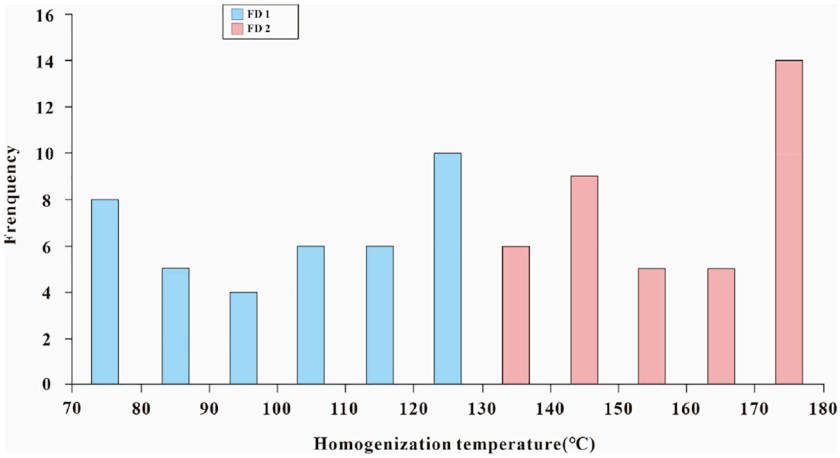

FIGURE 9
Histogram showing the ranges of homogenization temperatures of the fluid inclusions from filling dolomite (FD1 and FD2). Th=homogenization temperature.

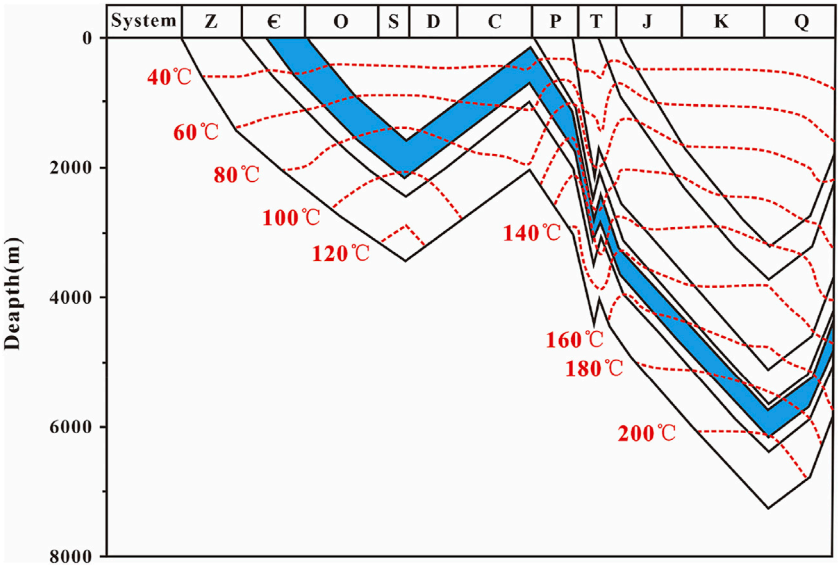

FIGURE 10
Typical burial and paleo-temperature history constructed from TH1 well from the eastern Sichuan Basin.

crystalline dolomite (MD 3-2, MD 3-3, MD 3–4) is later affected by hydrothermal fluids and thus should be attributed to burial dolomitization.

According to the above discussion, the genesis of the matrix dolomite in the Xixiangchi Formation of the study area seems to be the joint product of the early seepage reflux dolomitization and late burial dolomitization. Nonetheless, this research believes that the genesis of the matrix dolomite in the study area should be independent of burial dolomitization. Besides the evidence presented above, our opinion is also based on the following considerations:

To begin with, for almost all carbonate sediments, the burial process is associated with continuous diagenesis, which affects the carbon and oxygen isotopes of the matrix rock (Anderson and Arthur, 1983; Romanek et al., 1992; Prokoph et al., 2008). Determining the genesis of the ancient dolomite should not be completely based on the geochemical characteristics and instead should take other factors such as the geological setting and

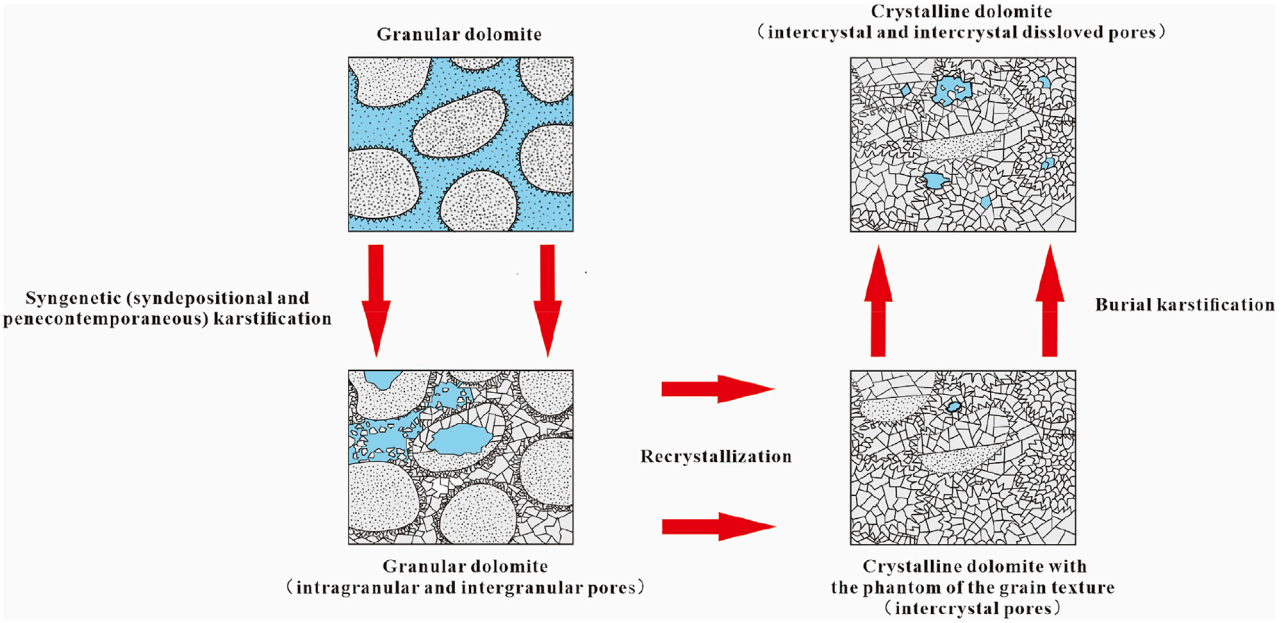

FIGURE 11
Formation and evolution model of the crystalline dolomite reservoirs in the Upper Cambrian Xixiangchi Formation in eastern Sichuan Basin (Modified from Yang et al., 2019).

principles of genesis into full consideration. Furthermore, the main mechanism behind burial dolomitization is that the mudstone in the basin produces Mg^{2+}-abundant fluids due to compaction, which flow into carbonate rock via the conduit such as faults and trigger dolomitization (Land, 1980; Kaufman and Knoll, 1995; Tang et al., 2006; Xu and Du, 2005). Assuming that the dolomite in the Xixiangchi Formation of the study area is affected by burial dolomitization, the key question lies in the source of the Mg^{2+} substance input that is sufficient to enable burial dolomitization. There is no development of extensive mudstone in the Xixiangchi Formation itself and the overlying Ordovician Tongzi Formation. The underlying Gaotai Formation, to some extent, develops mudstone, which, however, cannot facilitate the massive amount of Mg^{2+} required by the large-scale stratified dolomite occurring in the Xixiangchi Formation (Zhang X. F. et al., 2010; Jiang et al., 2015; Lei et al., 2015). Also, the gypsum-salt rock extensively develops in the Gaotai Formation (Jiang et al., 2015; Lei et al., 2015; Li et al., 2016). Consequently, it is safe to say that the source of Mg^{2+}-rich fluids in the Xixiangchi Formation in the study area is not the same as that of the Mg^{2+}-rich fluids required by burial dolomitization. At last, the REE evidence (∑REE) shows that in various matrix dolomite (MD) of the study area, the ∑REE values are below 100×10^{-6} and yet above 1×10^{-6}, with no positive anomaly of ∑REE. Previous studies conclude that the total REE content (∑REE) of the marine carbonate rock should be $(1–100) \times 10^{-6}$, and the carbonate rock affected by hydrothermal fluids should present a positive anomaly of the ∑REE value (Mclennan, 1989; Derry et al., 1994; Lei et al., 2016). Thus, the fluid source for dolomitization of the Xixiangchi Formation in the study area should be seawater (Hu et al., 2010; Lei et al., 2016; Liu et al., 2017). In addition, the various matrix dolomite (MD) in the Xixiangchi Formation of the study area is generally characterized by concentration of LREE and loss of HREE, associated with positive Ce anomaly (Figure 7). These also demonstrate that the diagenetic fluid for the matrix dolomite (MD) in the study water is seawater (Hu et al., 2010; Lei et al., 2016; Liu et al., 2017).

Based on the above discussion, this research believes that the mechanism behind dolomitization in the Xixiangchi Formation of the study area should be early evaporation concentration and seepage reflux, and the characteristics of burial dolomitization, presented by some matrix dolomite (MD), should be phantom induced by diagenesis (Figure 12).

For the dolomite reservoirs in the Xixiangchi Formation of the study area, dolomitization not only leads to the wide distribution of dolomite but also provides the bottommost basis for the formation and evolution of reservoir rock. It also significantly enhances the permeability of reservoir rock (Jardine and Wilshart, 1987; Ehrenberg, 2004; Ehrenberg et al., 2006). Dolomite is more brittle than limestone and thus more prone to cracking when externally loaded (Halley and Schmoker, 1983; Saller et al., 2004). In particular, with relatively deep burial depth, effective fractures in dolomite development are superior to that

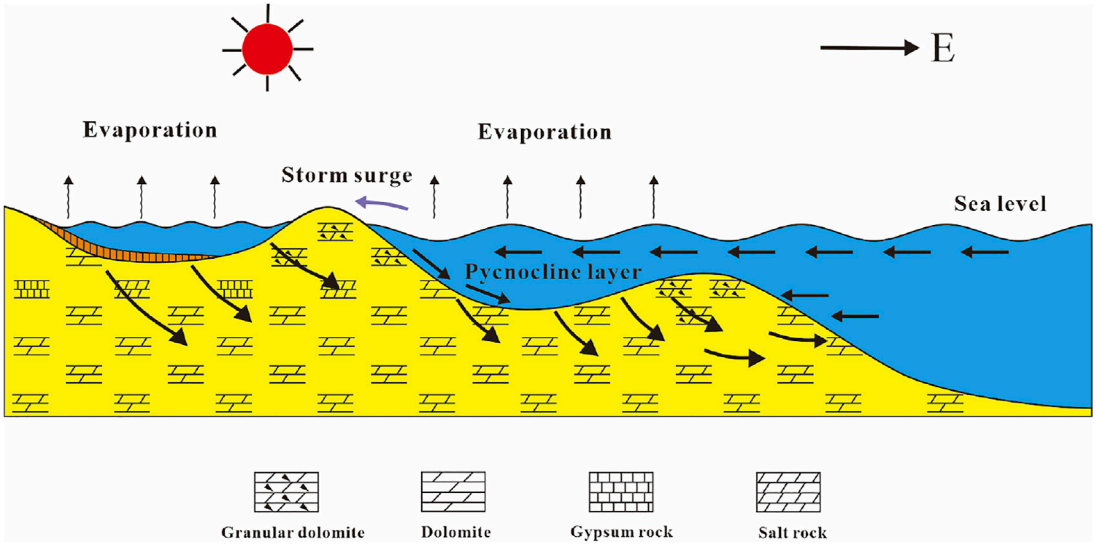

FIGURE 12
Dolomization model of Xixiangchi Formation (Modified from Yang et al., 2019). The mechanism behind dolomitization in the Xixiangchi Formation of the study area should be early evaporation concentration and seepage reflux, and the characteristics of burial dolomitization, presented by some matrix dolomite, should be phantom induced by diagenesis.

in limestone (Morrow, 1982; Murray, 1960; Warren, 2000; Ehrenberg et al., 2006). These fractures can serve as good flow channels and greatly enhance permeability (Jardine and Wilshart, 1987; Amthor et al., 1994; Sun, 1995; Li et al., 2019). Also, buried strata are all subjected to compaction, reducing porosity. Yet, dolomite presents relatively good compaction-resistant performance, which to some degrees offsets pore shrinkage and helps to maintain porosity and permeability. Therefore, it is considered that dolomitization is the essential diagenetic process for reservoir rock formation and evolution in the study area.

5.4 Karstificaiton and its impact on reservoir formation

During its deposition, the Xixiangchi Formation was subjected to multiple stages of karstification under paleogeomorphology, sedimentary environment, and tectonic movement. The karstification process in the Xixiangchi Formation of the study area is divided into the syngenetic (syndepositional and penecontemporaneous) and burial karstification stage based on the timing, product, and characteristics of karstification (Figure 13).

The fibrous cement in the granular dolomite is observed with partial dissolution and unconformity with the cement of the other stages. The fibrous cement is the product of early seabed cementation, and thus the dissolution of the fibrous cement and dissolution unconformity with the cement of other stages indicate that karstification occurs relatively early, supposedly between the first stage of seabed cementation and the second cementation stage (Hu et al., 2020; Shan et al., 2021; Fan et al., 2020; Li 2022). In other words, soon after deposition and short-term seabed cementation, the sediments experienced dissolution. The corresponding karstification is the syngenetic (syndepositional and penecontemporaneous) karstification.

Besides cement, pores and fractures are also affected by dissolution, which is mainly manifested in the following observations. First, some pores have harbor-like edges. Second, some pores are filled by bitumen, and they mostly present themselves as lining or streamer-like occurrence; the phenomenon of late granular cement dolomite (CD 2) dyed by bitumen is observed; some pores are seen with no filling of bitumen and thus clean pore space, and yet intensively dissolved dolomite crystals in the surrounding. Third, the structurally-induced fractures are expanded by dissolution (Figure 4F), and some fractures are bead-like. The above characteristics suggest that the study area is subjected to another karstification process, which should be later than the syngenetic one. We tend to interpret this later karstification as the burial karstification. Suppose the formation was subjected to supergene karstification. In that case, the study area should develop large-scale dissolution unconformity and the typical products of supergene karstification such as weathering crust, karst breccia, and grape-laced dolomite (Xu and Du, 2005; Yang et al., 2008; Hao et al., 2017; Yang et al., 2019; Yang X. F.

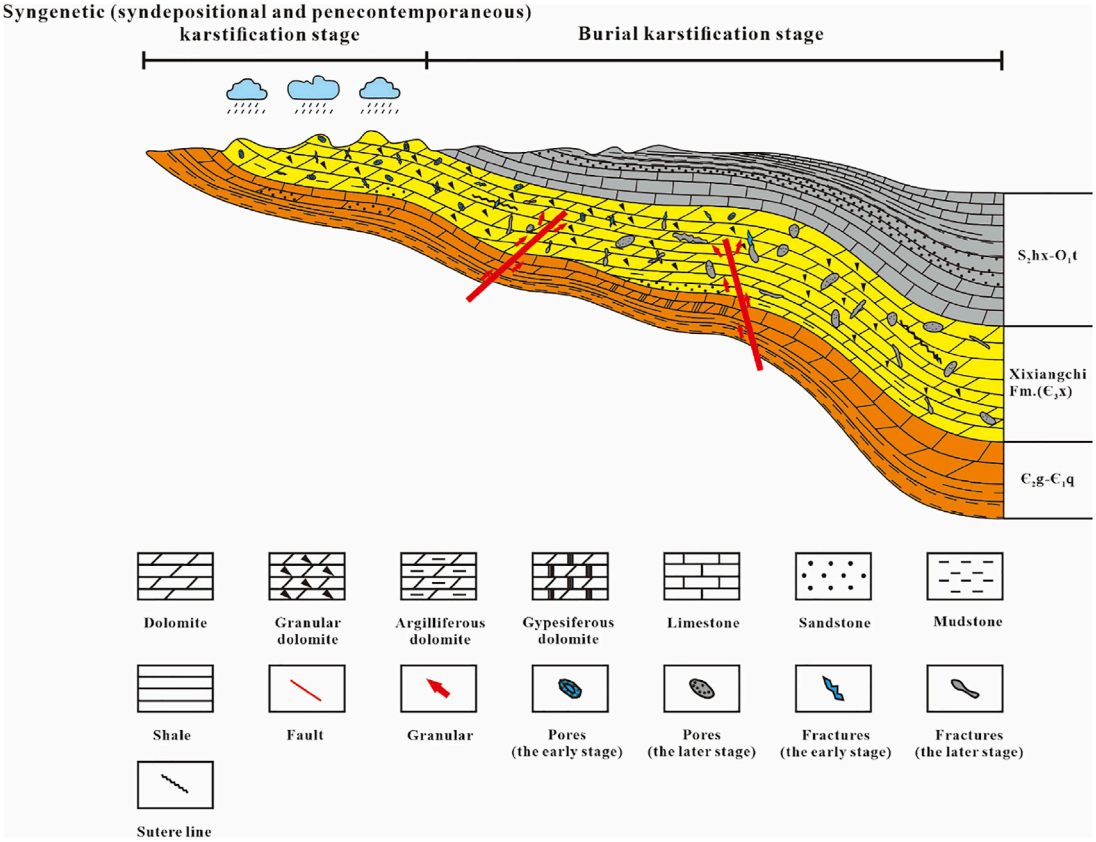

FIGURE 13
Karstification model of Xixiangchi Formation. Karstification results in new reservoirs space and re-adjustment of the early-formed reservoirs space and its position. Modified according to Li et al. (Li et al., 2020).

et al., 2019). However, such direct evidence is not found in the study area. Furthermore, the occurrence of bitumen demonstrates that the corresponding karstification is associated with the burial environment instead of the meteoric water environment.

The varied karstification stages are mainly dominated and differentiated by the different acid fluids (Sassen and Moore, 1988; Worden and Smalley, 1996; Xu and Du, 2005; Hao et al., 2017). On the one hand, the acid fluid of the syngenetic karstification originates from CO_2-rich meteoric water. On the other hand, the sources of the acid fluid for burial karstification are complicated—organic matter maturation, thermal sulfate reduction (TSR), and deep hydrothermal fluids can all generate acid fluids (Krouse et al., 1988; Sassen and Moore, 1988; Worden and Smalley, 1996; Davies and Smith, 2006; Zhu et al., 2006; Hu et al., 2009). We believe that the acid fluid for the burial karstification in the study area is derived from organic matter maturation, as directly implied by bitumen occurring in the dissolved pore. The organic matter at the maturation stage releases a large number of acid fluids containing corrosive components such as organic acid and CO_2, which enter and dissolve the reservoir rock before hydrocarbon charging (Krouse et al., 1988; Zhu et al., 2006; Hu et al., 2009) As the liquid hydrocarbon later flows into the pore and degrades, the resultant residual bitumen is preserved in the pore. With the increasing burial depth, crude oil cracking again generates acid fluids containing corrosive components, further dissolving the reservoir rock (Davies and Smith, 2006; Hu et al., 2009; Li et al., 2016; Li et al., 2019; He et al., 2021). The main product of crude oil cracking is natural gas; thus, no bitumen filling occurs in the dissolved pore. Nonetheless, in the case of deep burial, TSR, referring to the conversion of the sulfate into the acid fluids such as H_2S and CO_2 by hydrocarbons at high temperatures, can also generate acid fluids containing corrosive components. The onset of TSR requires three essential conditions, namely sufficient hydrocarbons, elevated temperatures (>120°C) and the development of thin gypsum rock (Worden and Smalley, 1996; Zhu et al., 2006). Although these three essential conditions are met in the study area, no direct evidence is found to support the onset of TSR, such as the development of secondary calcite in the gypsum moldic pore, pyrite crystals occurring at the interface between the gypsum, and secondary calcite, and presence of

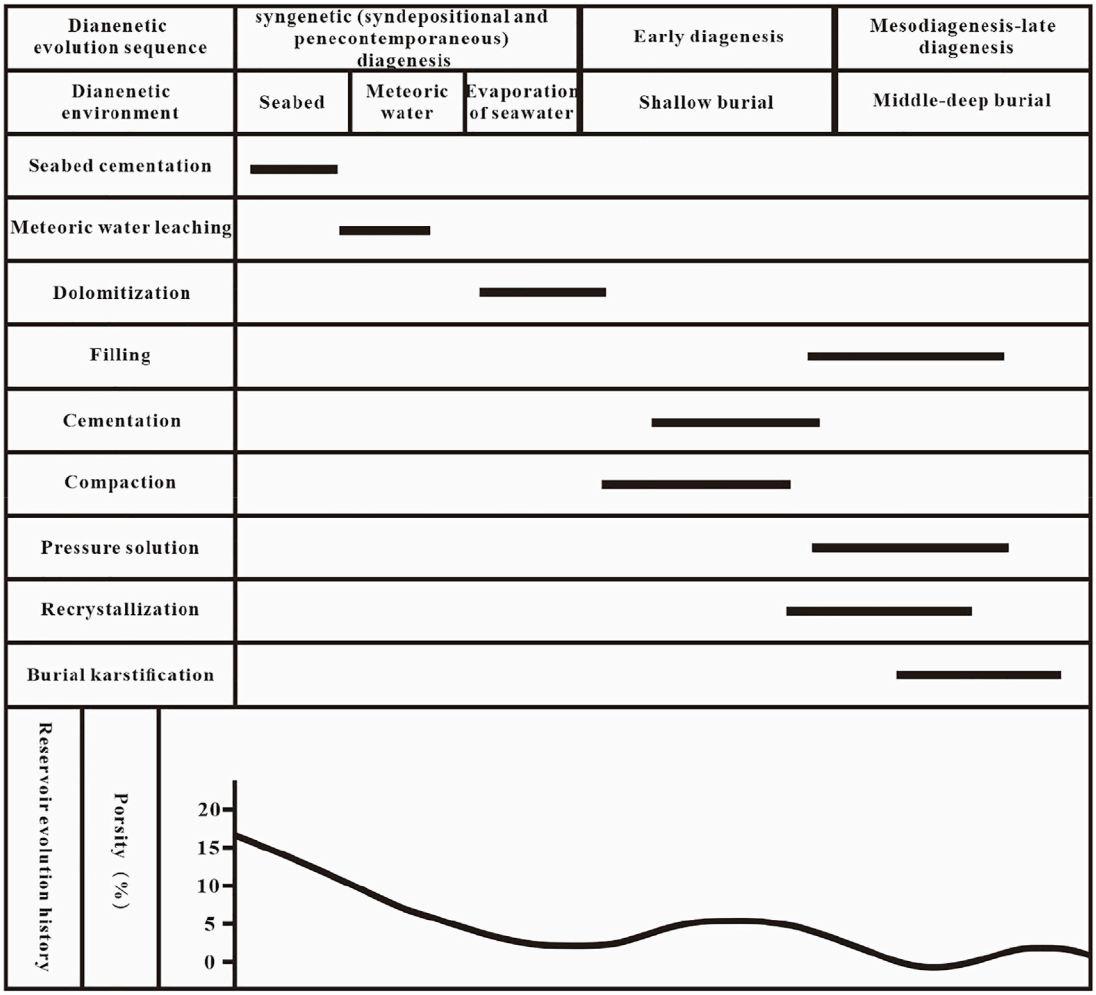

FIGURE 14
Evolution of diagenetic system in deep dolomite reservoirs of Xixiangchi Formation in the eastern Sichuan Basin.

high-H_2S natural gas (Krouse et al., 1988; Zhu et al., 2008). Dissolution by deep hydrothermal fluids typically occurs in fractures and dissolved pores and caves; thus, it is difficult to identify hydrothermal fluid dissolution traces from the resultant dissolution characteristic. Nonetheless, deep hydrothermal fluids may precipitate as they flow or due to variation in the formation temperatures, which produces typical hydrothermal minerals such as dolomite, quartz, fluorite, sphalerite, barite, and anhydrite (Davies and Smith, 2006; Zhu et al., 2008). The study area is seen with no development of such typical hydrothermal minerals, and thus the dissolution and alteration of the dolomite by hydrothermal fluids in the study area cannot be proved.

During the syngenetic (syndepositional and penecontemporaneous) stage, the sediments in the study area are subjected to cyclic exposure to the atmosphere due to sea level eustacy and also short-term leaching by meteoric water (Lin et al., 2017; Shi et al., 2020; Jia et al., 2021). During this stage, the sediments are in a semi-consolidated state (ductile–semi-ductile), and meteoric water leaching leads to selective dissolution, generating moldic pores, intragranular pores, and small dissolution fractures (Liu et al., 2017). However, meteoric water dissolution of this stage mainly occurs in the flat tidal deposition of relatively shallow water and intra-platform shoal deposition at the higher sedimentary terrain. Thus, the dissolution scale is small, and only a small quantity of dissolved pores are formed, mostly filled or damaged, due to later compaction, cementation, and filling. As the sediments reach a certain depth, burial dissolution leads to not only re-adjustment of the position of the reservoirs storage space but also occurrences of many new storage space types. As discussed above, burial karstification mainly occurs in the pore space of the early pores, caves, and fractures. In the granular and crystalline

dolomite, it primarily modifies the inner crystal and granular pores. The acid fluid migrates via fault and the early-formed pores, during which a large quantity of these pores are dissolved and re-adjusted to generate inter crystal dissolved pores, intergranular dissolved pores, and karst caves. Furthermore, such acid fluids may also flow through fractures or suture lines, dissolving the surrounding of the fracture wall and resulting in the bead-shaped dissolution-expanded fracture. Due to dissolution during the burial process, some isolated dissolved pores, karst caves, and dissolved fractures can also be effectively connected, which greatly enhances reservoir permeability.

In general, karstification results in new reservoirs space and re-adjustment of the early-formed reservoirs space and its position. It improves the porosity and permeability of the reservoir rock and thus enhances the reservoir's capacity. Therefore, karstification is considered a major factor affecting the reservoir's capacity.

5.5 Diagenetic evolution and its impact on reservoir formation

Based on the above analysis and the impact of diagenesis on the reservoirs, the diagenetic stages of the Xixiangchi Formation in the Sichuan Basin can be divided into the following stages (Figure 14).

During the syngenetic (syndepositional and penecontemporaneous) diagenesis stage, thick granular rocks featuring the highest deposit of water body energy and many developed intergranular pores normally accumulate in highland. A small number of secondary pores were formed easily under the syngenetic (syndepositional and penecontemporaneous) karstification. Also, the original intergranular porosity is low, with fine sediments on bottom lands between beaches. The primary porosity is reduced by 10–20% due to the deposited granular rock cemented by the early-formed fibrous cement under the sea. Meanwhile, micrite dolomite forms from the micrite calcite under the effect of dolomitization related to evaporation concentration and seepage reflux, of which the intercrystalline pores are highly developed, roughly above 50% (Figure 14).

During the early diagenesis stage, the sediments formed in the previous stage enter the shallow burial environment along with the deposition of the overlying formation. And porosities of intergranular and intercrystalline pores are reduced by 35–40% under the influence of compaction. Further, the cementation in the shallow burial stage promotes the disappearance of the storage space. Granular dolomite cement caused porosity loss of 20–25% and left some isolated intergranular pores and intercrystalline pores. In the meantime, dolomite crystals become thicker and form into powder-fine crystalline dolomite under the effect of recrystallization related to the buried depth. Also, the retained intercrystalline pores are readjusted and optimized. In effect, the recrystallization outcome increases the rock's effective porosity and permeability to a certain extent.

In the mesodiagenesis-late diagenesis stage, the recrystallization intensity grows with the rising burial depth, and the intercrystalline pores are constantly adjusted and optimized. Besides, pressure solution starts to occur and results in the suture line structure. When the burial depth reaches a certain value, the organic matter in the underlying Qiongzhusi Formation mudstone gradually transforms into liquid and gaseous hydrocarbons. And the occurrence of burial karstification is triggered by the large number of organic acids produced during the maturation of hydrocarbons. Buried karst can also form certain amounts of new pores to increase the porosity apart from modifying and adjusting the remaining intercrystalline and intergranular pores (Wang and Wang, 2021). What's more, some isolated dissolution pores, caves, and dissolution fractures can be effectively connected, greatly enhancing the permeability of the reservoir. The effective porosity can still reach 2–5%, although the porosity has decreased with the emergence of bitumen and dolomite fillings.

6 Conclusion

According to the petrographic characteristics, crystalline dolomite reservoirs dominated by crystalline dolomite and granular dolomite reservoirs dominated by granular dolomite are mainly developed in the Xixiangchi Formation. The formation was extremely vulnerable to various diagenesis during the geological history of deposition and burial for the long history of sedimentary time, and the dolomite was strongly sensitive to the diagenetic environment. The syngenetic (syndepositional and penecontemporaneous) diagenesis, the early diagenesis, and the mesodiagenesis-late diagenesis are three stages in the diagenetic process of deep dolomite reservoirs in the study area based on petrographic characteristics, geochemical characteristics, and burial history.

During the syngenetic (syndepositional and penecontemporaneous) diagenesis stage, dolomitization is closely related to evaporation concentration, and seepage reflux of high-salinity seawater facilitates the reservoir rock development by greatly enhancing the reservoir rock permeability. At the same time, Syngenetic karstification generates a small number of secondary pores in the sediments of the grain shoal facies via selective dissolution, and yet such primary pores are destructed by the cement early formed in the seabed diagenetic environment. In the early diagenesis stage, compaction and second-stage cementation further led to the disappearance of primary pores. Yet the dolomite and cement, to some extent, support the rock framework and thus resist compaction, which somewhat helps to preserve the primary

pores. The formation of the crystalline dolomite reservoir rock is mainly attributed to recrystallization, which to some degree alters the pore structure of the original rock and increases the effective porosity. In this regard, recrystallization facilitates the later modification of reservoir rock by karstification. A decrease in porosity is increased with the appearance of dolomite filling and bitumen in the mesodiagenesis-late diagenesis stage. Filling, cementation, and compaction are the main reasons for the decline of reservoir pores. The diagenetic system is in an enclosed environment with increasing burial depth. The burial karstification related to acidic fluids starts to appear. Then, the previously formed reservoir space and the reservoir position were re-adjusted, increasing the reservoir's porosity and permeability. It is a major contributor to enhancing reservoir capability and forming effective reservoir space.

According to the study of the Xixiangchi Formation of the study area, the influence of diagenesis on deep dolomite reservoirs is not caused by one or several types of diageneses. Instead, different diageneses in various diagenetic periods affect the reservoir. What's more, the strength of diagenesis also influences various reservoirs differently.

Data availability statement

The original contributions presented in the study are included in the article/supplementary material, further inquiries can be directed to the corresponding author.

Author contributions

GR, QQ, and ZQ contributed in writing, reviewing, and editing, datacuration, writing original draft preparation; YG and CY contributed in formal analysis, validation, and reviewing.

Funding

This study was financially supported by Comprehensive exploration research project of PetroChina Southwest Oil; Gas Field Company in 2020 (Grant No. XNS02J2020-0050), Project funded by Major Science and Technology Project of CNPC (Grant No. 2016E10-0611), "13th five year plan" National Science and Technology Major Project (Grant No. 2016ZX05062), and National Natural Science Foundation (Grant No. 41402126).

Acknowledgments

PetroChina Southwest Oil & Gas Field Company is thanked for providing basic data. Minglong Li in Southwest Petroleum University is thanked for helping analyze stable isotopes. Fei Li in Southwest Petroleum University assisted with situ LA-ICP-MS analysis.

Conflict of interest

The authors ZQ, YG and ZY are employed by Southwest Oil and Gas Field Company, Petro China.

The remaining authors declare that the research was conducted in the absence of any commercial or financial relationships that could be construed as a potential conflict of interest.

Publisher's note

References

Amthor, J. E., Mountjoy, E. W., and Machel, H. G. (1994). Regional-scale porosity and permeability variations in Upper Devonian Leducbuildups: Implications for reservoirs development and prediction in carbonates. *AAPG Bull.* 78 (10), 1541–1559. doi:10.1306/A25FF215-171B-11D7-8645000102C1865D

Anderson, T., and Arthur, M. A. (1983). Stable isotopes of oxygen and carbon and their application to sedimentologic and paleonvironmental problems. *SEPM Short. Course* 10, 1–151. doi:10.2110/scn.83.01.0000

Badiozamani, K. (1973). The dorag dolomitization model-application to the middle ordovician of sisconsin. *J. Sediment. Petrology* 43 (4), 965–984. doi:10.1306/74D728C9-2B21-11D7-8648000102C1865D

Bai, G. P., and Cao, B. F. (2014). Characteristics and distribution patterns of deep petroleum accumulations in the world. *Oil Gas Geol.* 35 (1), 19–25. doi:10.11743/ogg20140103

Davies, G. R., and Smith, L. B. (2006). Structurally controlled hydrothermal dolomite reservoir facies: An overview. *Am. Assoc. Pet. Geol. Bull.* 90 (11), 1641–1690. doi:10.1306/05220605164

Deng, K. L. (1992). Formation and evolution of Sichuan Basin and domains oil and gas exploration. *Nat. Gas. Ind.* 12 (5), 7–13.

Derry, L, A., Brasier, M. D., Corfield, R. M., Rozanov, A. Y., and Zhuravlev, A. Y. (1994). Sr and C isotopes in Lower Cambrian carbonates from the Siberian craton:A paleoenvironmental record during the 'Cambrian explosion. *Earth Planet. Sci. Lett.* 128 (3-4), 671–681. doi:10.1016/0012-821x(94)90178-3

Dyman, T. S., Crovelli, R. A., Bartberger, C. E., and Takahashi, K. I. (2002). Worldwide estimates of deep natural gas resources based on the U.S. *Nat. Resour. Res.* 11 (3), 207–218. doi:10.1023/a:1019860722244

Ehrenberg, S. N., Eberli, G. P., Keramati, M., and Moallemi, S. A. (2006). Porosity-permeability relationships in interlayered limestone-dolostone reservoirs. *Am. Assoc. Pet. Geol. Bull.* 90 (1), 91–114. doi:10.1306/08100505087

Ehrenberg, S. N. (2004). Factors controlling porosity in upper carboniferous–lower permian carbonate strata of the barents sea. *Am. Assoc. Pet. Geol. Bull.* 88 (12), 1653–1676. doi:10.1306/07190403124

Fan, C. H., Li, H., Qin, Q. R., He, S., and Zhong, C. (2020). Geological conditions and exploration potential of shale gas reservoir in Wufeng and Longmaxi

Formation of southeastern Sichuan Basin, China. *J. Petroleum Sci. Eng.* 191, 107138. doi:10.1016/j.petrol.2020.107138

Fan, C. H., Li, H., Zhao, S. X., Qin, Q. R., Fan, Y., Wu, J. F., et al. (2020). Formation stages and evolution patterns of structural fractures in marine shale: Case study of the Lower Silurian Longmaxi Formation in the Changning area of the Southern Sichuan Basin, China. *Energy Fuels* 34 (8), 9524–9539. doi:10.1021/acs.energyfuels.0c01748

Fan, C. H., Xie, H. B., Li, H., Zhao, S. X., Shi, X. C., Liu, J. F., et al. (2022). Complicated fault characterization and its influence on shale gas preservation in the southern margin of the Sichuan Basin, China. *Lithosphere* 2022, 8035106. doi:10.2113/2022/8035106

Fang, S. X., Hou, F. H., and Dong, Z. X. (2003). Non-stromatoltite ecologic system cyanobacteria dolostone in Dengying Formation of Upper-Sinian. *Acta Sedimentol. Sin.* 21 (1), 96–102.

Feng, Z. Z., Peng, Y. M., Jin, Z. K., and Bao, Z. D. (2002). Lithofacies palaeogeography of the late Cambrian in China. *J. Palaeogeogr.* 4 (3), 1–10. doi:10.7605/gdlxb.2004.02.001

Fu, J. H., Fan, L. Y., Liu, X., and Huang, D. J. (2019). Gas accumulation conditions and key exploration & development technologies in Yuanba gas field. *Acta Pet. Sin.* 40 (2), 748–760. doi:10.7623/syxb201902013

Gao, F. Q. (2019). Use of numerical modeling for analyzing rock mechanic problems in underground coal mine practices. *J. Min. Strata Control Eng.* 1 (1), 013004. doi:10.13532/j.jmsce.cn10-1638/td.2019.02.009

Halley, R. B., and Schmoker, J. W. (1983). High-porosity cenozoic carbonaterocks of South Florida: Progressive loss of porosity with depth. *AAPG Bull.* 67 (2), 191–200. doi:10.1306/03B5ACE6-16D1-11D7-8645000102C1865D

Hao, Y., Yang, X., Wang, Y. F., Chen, W., Gu, M. F., and Hou, G. F. (2017). Supergene karstification in the sinian dengying formation, Sichuan basin. *Sediment. Geol. Tethyan Geol.* 37 (1), 48–54.

He, D. F., Li, D. S., Zhang, G. W., Zhao, L. Z., Fang, C., Lu, R. Q., et al. (2011). Formation and evolution of multi-cycle superposed Sichuan Basin, China. *Chin. J. Geol.* 46 (3), 589–606.

He, S., Li, H., Qin, Q. R., and Long, S. X. (2021). Influence of mineral compositions on shale pore development of Longmaxi Formation in the Dingshan area, southeastern Sichuan Basin, China. *Energy Fuels* 35 (13), 10551–10561. doi:10.1021/acs.energyfuels.1c01026

He, Z. L., Jin, X. H., Wo, Y. J., Li, H. L., Bai, Z. R., Jiao, C. L., et al. (2016). Hydrocarbon accumulation characteristics and exploration domains of ultra-deep marine carbonates in China. *China Pet. Explor.* 21 (1), 3–14. doi:10.3969/j.issn.1672-7703.2016.01.001

He, Z. L., Zhang, J. T., Ding, Q., You, D. H., Peng, S. T., Zhu, D. Y., et al. (2017). Factors controlling the formation of high-quality deep to ultra-deep carbonate reservoirs. *Oil Gas Geol.* 38 (4), 633–644. doi:10.11743/ogg20170401

Hu, M. Y., Cai, X. Y., Hu, Z. G., Qian, Y., and Xiang, J. (2009). Deep buried dissolution of ordovician carbonates in tazhong area of Tarim Basin. *J. Oil Gas Technol. (JJPI)* 31 (6), 49–54.

Hu, W. X., Chen, Q., Wang, X. L., and Cao, J. (2010). REE models for the discrimination of fluids in the formation and evolution of dolomite reservoirs. *Oil Gas Geol.* 31 (6), 810–818. doi:10.11743/ogg20100614

Hu, Y. J., Cai, C. F., Liu, D. W., Chelsea, L. P., Jiang, L., Shen, J. A., et al. (2020). Formation, diagenesis and palaeoenvironmental significance of upper Ediacaran fibrous dolomite cements. *Sedimentology* 67, 1161–1187. doi:10.1111/sed.12683

Jardine, D., and Wilshart, J. W. (1987). Carbonate reservoirs description(in reservoirs sedimentology). *Soc. Econ. Paleontolo-gists Mineralogists* 40, 129–152. doi:10.2110/pec.87.40.0129

Jia, C. Z., and Pang, X. Q. (2015). Research process and development directions of deep hydrocarbon geological theories. *ACTA Pet. Sin.* 36 (12), 1457–1469. doi:10.7623/syxb201512001

Jia, P., Huang, F. X., Lin, S. G., Song, T., Gao, Y., Lv, W. N., et al. (2021). Sedimentary facies and model characteristics of middle upper cambrian Xixiangchi group in sichuang basin and its adjacent areas. *Geoscience* 35 (4), 1–12. doi:10.19657/j.geoscience.1000-8527.2021.026

Jiang, X. Q., Guan, H. L., Liu, G. X., Li, J. M., Luo, K. P., Yan, J. X., et al. (2015). Diagenesis of middle and upper cambrian loushanguan group reservoirs in nanchuan area, Sichuan basin. *Petroleum Geol. Experriment* 37 (3), 314–319. doi:10.11781/sysydz201503314

Jiao, F. Z., Feng, J. H., Yi, J. Z., Cai, X. Y., and He, F. Q. (2015). Direction, key factors and solution of marine natural gas exploration in Yangtze area. *China Pet. Explor.* 20 (2), 1–8. doi:10.3969/j.issn.1672-7703.2015.02.001

Jin, M. D., Li, B. S., Zhu, X., Dai, L. C., Jiang, Z. L., Wu, H., et al. (2020). Characteristics and main controlling factors of reservoirs in the fourth member of Sinian Dengying Formation in Yuanba and its peripheral area, northeastern Sichuan Basin, SW China. *Petroleum Explor. Dev.* 47 (6), 1172–1182. doi:10.1016/s1876-3804(20)60127-1

Kaufman, A. J., and Knoll, A. H. (1995). Neoproterozoic variations in the C-isotopic composition of seawater:stratigraphic and biogeochemical implications. *Precambrian Res.* 73 (1-4), 27–49. doi:10.1016/0301-9268(94)00070-8

Krouse, H. R., Viau, C. A., Eliuk, L. S., Ueda, A., and Halas, S. (1988). Chemical and isotopic evidence of thermochemical sulphate reduction by light hydrocarbon gases in deep carbonate reservoirs. *Nature* 33 (2), 415–419. doi:10.1038/333415a0

Land, L. S. (1980). "The isotopic and minor element geochemistry of dolomite: The state of the art," in *Concepts and models of dolomitization*. Editors D. H. Zenger, J. B. Dunham, and R. L. Ethington (Tulsa, Oklahoma: SEPM, Special publication) 28, 87–110.

Lei, H. J., Li, G. R., Gao, Y. W., Zhou, J. L., Feng, Y. Y., Fu, H., et al. (2016). Geochemical characteristics and generation mechanism of cambrian dolomite in the south of Sichuan basin. *Mar. Orig. Pet. Geol.* 21 (3), 39–47. doi:10.7623/syxb201609004

Lei, H. J., Li, G. R., Zhou, J. L., Gao, Y. W., Shen, T., Fu, H., et al. (2015). Carbonate diagenesis feature and controlling over reservoirs of Cambrian in south area of Sichuan Basin. *J. Northeast Petroleum Univ.* 39 (2), 59–68. doi:10.3969/j.issn.2095-4107.2015.02.008

Li, H. K., Li, Z. Q., Long, W., Wan, S. S., Ding, S., Wang, S. Z., et al. (2019a). Vertical configuration of Sichuan Basin and its superimposed characteristics of the prototype basin. *J. Chengdu Unniversity Technol. Technol. Ed.* 46 (3), 257–267. doi:10.3969/j.issn.1671-9727.2019.03.01

Li, H., Qin, Q. R., Zhang, B. J., Ge, X. Y., Hu, X., Fan, C. H., et al. (2020). Tectonic fracture Formation and distribution in ultradeep marine carbonate gas reservoirs: A case study of the maokou Formation in the jiulongshan gas field, Sichuan basin, southwest China. *Energy fuels.* 34 (11), 14132–14146. doi:10.1021/acs.energyfuels.0c03327

Li, H. (2022). Research progress on evaluation methods and factors influencing shale brittleness: A review. *Energy Rep.* 8, 4344–4358. doi:10.1016/j.egyr.2022.03.120

Li, H., Tang, H. M., Qin, Q. R., Zhou, J. L., Qin, Z. J., Fan, C. H., et al. (2019). Characteristics, formation periods and genetic mechanisms of tectonic fractures in the tight gas sandstones reservoir: A case study of xujiahe Formation in YB area, Sichuan basin, China. *J. Petroleum Sci. Eng.* 178, 723–735. doi:10.1016/j.petrol.2019.04.007

Li, H., Wang, Q., Qin, Q. R., and Ge, X. Y. (2021b). Characteristics of natural fractures in an ultradeep marine carbonate gas reservoir and their impact on the reservoir: A case study of the maokou formation of the jls structure in the Sichuan basin, China. *Energy fuels.* 35 (16), 13098–13108. doi:10.1021/acs.energyfuels.1c01581

Li, H., Tang, H. M., and Zheng, M. J. (2019). Micropore structural heterogeneity of siliceous shale reservoir of the Longmaxi Formation in the southern Sichuan Basin, China. *Minerals* 9, 548. doi:10.3390/min9090548

Li, H., Tang, H. M., Qin, Q. R., Wang, Q., and Zhong, C. (2019). Effectiveness evaluation of natural fractures in Xujiahe Formation of Yuanba area, Sichuan basin, China. *Arabian J. Geosci.* 12 (6), 194. doi:10.1007/s12517-019-4292-5

Li, H. T., Peng, R., Du, W. S., Li, X. P., and Zhang, N. B. (2021c). Experimental study on structural sensitivity and intervention mechanism of mechanical behavior of coal samples. *J. Min. Strata Control Eng.* 3(4), 043012. doi:10.1021/acsomega.1c05077

Li, J., He, D. F., Du, Y., Cui, J., Ma, Y., and Zhang, X. (2014). Electroacupuncture improves cerebral blood flow and attenuates moderate ischemic injury via Angiotensin II its receptors-mediated mechanism in rats. *BMC Complement. Altern. Med.* 16 (4), 441–460. doi:10.1186/1472-6882-14-441

Li, J., Li, H., Yang, C., Wu, Y. J., Gao, Z., and Jiang, S. L. (2022). Geological characteristics and controlling factors of deep shale gas enrichment of the Wufeng-Longmaxi Formation in the southern Sichuan Basin. *China. Lithosphere*, 2022. 4737801. doi:10.2113/1970/4737801

Li, J., Li, H., Xu, J. L., Wu, Y. J., and Gao, Z. (2022). Effects of fracture formation stage on shale gas preservation conditions and enrichment in complex structural areas in the southern Sichuan Basin, China. *Frontiers in Earth Sci.*, 9. 823855. doi:10.3389/feart.2022.921988

Li, J. Z., Tao, X. W., Bai, B., Huang, S. P., Jiang, Q. C., Zhao, Z. Y., et al. (2021). Geological conditions, reservoirs evolution and favorable exploration directions of marine ultra-deep oil and gas in China. *Petroleum Explor. Dev.* 48 (1), 52–67. doi:10.1016/S1876-3804(21)60005-8

Li, W. Z., Zhou, J. G., Zhang, J. Y., Hao, Y., Zeng, Y. Y., Wang, F., et al. (2016). Main controlling factors and favorable zone distribution of Xixiangchi Formation reservoirs in the Sichuan Basin. *Nat. Gas. Ind.* 36 (1), 52–60. doi:10.3787/j.issn.1000-0976.2016.01.006

Li, W. Z., Wen, L., Gu, M. F., Xia, M. L., Xie, W. R., Fu, X.D.,, et al. (2020). Development models of Xixiangchi Formation karst reservoirs in the Late Caledonian in the central Sichuan Basin and its oil-gas exploration implications. *Nat. Gas. Ind.* 40 (9), 30–38. doi:10.3787/j.issn.1000-0976.2020.10.004

Li, Z. Q., Ying, D. L., Li, H. K., Yang, G., Zeng, Q., Guo, X. Y., et al. (2011). Evolution of the Western Sichuan basin and its superimposed characteristics, China. *Acta Petrol. Sin.* 27 (8), 2362–2370.

Lin, X. X., Peng, J., Yan, J. P., and Hou, Z. J. (2015). A discussion about origin of botryoidal dolostone of the sinian dengying Formation in Sichuan Basin. *J. Palaeogeogr.* 17 (6), 755–770. doi:10.7605/gdlxb.2015.06.062

Lin, Y., Chen, C., Shan, S. J., Zeng, Y. Y., Liu, X., and Chen, Y. L. (2017). Reservoirs characteristics and main controlling factors of the cambrian Xixiangchi Formation in the Sichuan basin. *Petroleum Geol. Exp.* 39 (5), 610–616. doi:10.11781/sysydz201705610

Liu, C., Xie, Q. B., Wang, G. W., He, W. G., Song, Y. F., Tang, Y., et al. (2017). Rare Earth element characteristics of the carboniferous huanglong formation dolomites in eastern Sichuan basin, southwest China: Implications for origins of dolomitizing and diagenetic fluids. *Mar. Pet. Geol.* 81, 33–49. doi:10.1016/j.marpetgeo.2016.12.030

Liu, D. W., Cai, C. F., Hu, Y. J., Jang, L., Peng, Y. Y., Yu, R., et al. (2020). Multi-stage dolomitization process of deep burial dolostones and its influence on pore evolution: A case study of longwangmiao Formation in the lower cambrian of central Sichuan basin. *J. China Univ. Min. Technol.* 49 (6), 1150–1165. doi:10.1016/j.marpetgeo.2020.104752

Liu, L. H., Du, X. D., Xu, S. L., and Wen, H. G. (2017a). Characteristics and Formation of the cambrian dolomite in middle-south Sichuan basin, China. *J. Jilin Univ. Sci. Ed.* 47 (3), 775–784. doi:10.13278/j.cnki.jjuese.201703111

Liu, S. G., Deng, B., Sun, W., Zhong, Y., Li, Z. W., Li, J. X., et al. (2018). Sichuan Basin:A superimposed sedimentary basin mainly controlled by its peripheric tectonics. *Chin. J. Geol.* 53 (1), 308–326. doi:10.12017/dzkx.2018.018

Liu, S. G., Li, Z. B., Sun, W., Deng, B., Luo, Z. L., Wang, G. Z., et al. (2011). Basin geological features of superimposed basin and hydrocarbon accumulation in Sichuan Basin, China. *Chin. J. Geol.* 46 (1), 233–257. doi:10.3969/j.issn.0563-5020.2011.01.019

Ma, X. H., Yang, Y., Wen, L., and Luo, B. (2019a). Distribution and exploration direction of medium- and large-sized marine carbonate gas fields in Sichuan Basin, SW China. *Petroleum Explor. Dev.* 46 (1), 1–15. doi:10.1016/s1876-3804(19)30001-1

Ma, Y. S., Cai, X. Y., Zhao, P. R., and Zhu, H. Q. (2011). The research status and advances in porosity evolution and diagenesis of deep carbonate reservoirs. *Earth Sci. Front.* 18 (4), 181–192.

Ma, Y. S., He, Z. L., Zhao, P. R., Zhu, H. Q., Han, J., You, D. H., et al. (2019). A new progress in foumation mechanism of deep and ultra-deep carbonate reservoirs. *Acta Pet. Sin.* 40 (12), 1414–1425. doi:10.7623/syxb201912001

Mckenzie, J. A. (1981). Holocene dolomitization of calcium carbonate sediments from the coastal sabkhas of abu dhabi, U.A.E. A stable isotope study. *J. Geol.* 89 (2), 185–198. doi:10.1086/628579

Mclennan, S. M. (1989). Rare Earth elements in sedimentary rocks: Influence of provenance and sedimentary process. *Rev. Mineralogy* 21, 169–200. doi:10.1515/9781501509032-010

Mitchell, J. M., Paul, A. B., and Stephen, J. B. (1996). Recrystallization of dolomite: an experimental study from. *Geochimica Cosmochimica Acta* 60 (12), 2189–2207. doi:10.1016/0016-7037(96)00062-2

Moor, C. H., and Druckman, Y. (1981). Burial diagenesis and porosity evolution, upper jurassic smackover, Arkansas and lonisana. *AAPG Bull.* 65 (4), 597–628. doi:10.1306/2F919995-16CE-11D7-8645000102C1865D

Morrow, D. W. (1982). Diagenesis 1: Dolomite-part 1, the chemistry ofdolomitization and dolomite precipitation. *Geosci. Can.* 9 (1), 5–13.

Murray, R, C. (1960). Origin of porosity in carbonate rocks. *J. Sediment. Petrology* 30 (1), 59–84. doi:10.1306/74D709CA-2B21-11D7-8648000102C1865D

Pang, X. Q. (2010). Key challenges and research methods of petroleum exploration in the deep of super imposed basins in Western China. *Oil Gas Geol.* 31 (5), 517–534. doi:10.11743/ogg20100501

Park, W. C., and Schot, E. H. (1968). Styloites, their nature and origin. *J. Sediment. Petrology* 38 (1), 1–175.

Prokoph, A., Shields, G. A., and Veizer, J. (2008). Compilation and time-series analysis of a marine carbonate $\delta^{18}O$, $\delta^{13}C$, $^{87}Sr/^{86}Sr$ and $\delta^{34}S$ database through Earth history. *Earth. Sci. Rev.* 87, 113–133. doi:10.1016/j.earscirev.2007.12.003

Qian, Y. X., Taberner, C., Zou, S. L., You, D. H., and Wang, R. Y. (2007). Diagenesis comparison between epigenic karstification and burial dissolution in carbonate reservoirs:An instance of Ordovician carbonate reservoirs in Tabei and Tazhong regions, Tarim Basin. *Mar. Orig. Pet. Geol.* 12 (2), 1–7. doi:10.3969/j.issn.1672-9854.2007.02.001

Qie, L., Shi, Y. N., and Liu, J. G. (2021). Experimental study on grouting diffusion of gangue solid filling bulk materials. *J. Min. Strata Control Eng.* 3 (2), 023011. doi:10.13532/j.jmsce.cn10-1638/td.20201111.001

Romanek, C. S., Grossman, E. L., and Morse, J. W. (1992). Carbon isotopic fractionation in synthetic aragonite and calcite: Effects of temperature and precipitation rate. *Geochimica Cosmochimica Acta* 56 (1), 419–430. doi:10.1016/0016-7037(92)90142-6

Saller, A. H., Walden, S., Robertson, S., Nims, R., Schwab, J., Hagiwara, H., et al. (2004). *Three-dimensional seismic imaging of an Upper Paleozoic "reefal" buildup, Reinecke field, west Texas, United States.* Oklahoma, United States: AAPG Memoir, 107–122.

Sassen, R., and Moore, C. H. (1988). Framework of hydrocarbon generation and destruction in eastern Smackovertrend. *AAPG Bull.* 72 (6), 649–663.

Shan, S. C., Wu, Y. Z., Fu, Y. K., and Zhou, P. H. (2021). Shear mechanical properties of anchored rock mass under impact load. *J. Min. Strata Control Eng.* 3 (4), 043034. doi:10.13532/j.jmsce.cn10-1638/td.20211014.001

Shen, A. J., Zhao, W. Z., Hu, A. P., She, M., Chen, Y. N., and Wang, X. F. (2015). Major factors controlling the development of marine carbonate reservoirs. *Petroleum Explor. Dev.* 42 (5), 597–608. doi:10.1016/s1876-3804(15)30055-0

Shi, S. Y., Wang, T. S., Liu, W., Jiang, H., Li, Q. F., Liu, X., et al. (2020). Reservoirs characteristic and gas exploration potential in cambrian Xixiangchi Formation of Sichuan basin. *Nat. Gas. Geosci.* 31 (6), 773–785. doi:10.11764/j.issn.1672-1926.2020.03.007

Sun, S. Q. (1995). Dolomite reservoirs:Porosity evolution and reservoirs characteristics. *AAPG Bull.* 79 (2), 186–204.

Tang, C. Y., Wang, M., Yao, H. Z., Duan, Q. F., and Zhao, X. L. (2006). Current topics about dolomitization and the problem of dolostones. *Jouranal East China Inst. Technol.* 29 (3), 205–210. doi:10.3969/j.issn.1674-3504.2006.03.002

Veizer, J., Ala, D., Azmy, K., Bruckschen, P., Buhl, D., Bruhn, F., et al. (1999). $^{87}Sr/^{86}Sr$, $\delta^{13}C$ and$\delta^{18}O$ evolution of Phanerozoic seawater. *Chem. Geol.* 161 (1-3), 59–88. doi:10.1016/s0009-2541(99)00081-9

Wang, J., and Wang, X. L. (2021). Seepage characteristic and fracture development of protected seam caused by mining protecting strata. *J. Min. Strata Control Eng.* 3 (3), 033511. doi:10.13532/j.jmsce.cn10-1638/td.20201215.001

Wang, Q. C., and Jin, Z. Y. (2002). Superimposed basin and oil-gas formation and accumulation. *Chin. Basic Sci.* 6, 4–7. doi:10.3969/j.issn.1009-2412.2002.06.001

Wang, S. L., Li, H., Lin, L. F., and Yin, S. (2022). Development characteristics and finite element simulation of fractures in tight oil sandstone reservoirs of Yanchang Formation in western Ordos Basin. *Frontiers Earth Sci.* 9, 823855. doi:10.3389/feart.2021.823855

Warren, J. (2000). Dolomite:Occurrence, evolution and economically important associations. *Earth. Sci. Rev.* 52 (1-3), 1–81. doi:10.1016/s0012-8252(00)00022-2

Wei, G. Q., Yang, W., Xie, W. R., Jin, H., Su, N., Sun, A., et al. (2018). Accumulation modes and exploration domains of Sinian-Cambrian natural gas in Sichuan Basin. *Acta Pet. Sin.* 39 (12), 1317–1327. doi:10.7623/syxb201812001

Worden, R. H., and Smalley, P. C. (1996). H_2S-producing reactions in deep carbonate gas reservoirs:Khuff Formation, Abu Dhabi. *Chem. Geol.* 133 (1-4), 157–171. doi:10.1016/s0009-2541(96)00074-5

Xu, X. S., and Du, B. W. (2005). The palaeoweathering crust -type karst reservoir rocks in carbonate rocks. *Sediment. Geol. TethyanGeology* 25 (3), 1–7. doi:10.3969/j.issn.1009-3850.2005.03.001

Yang, F., Zhang, H. A., Wang, X. J., Peng, J., Mo, J. W., Zhuo, S. Q., et al. (2019). Characteristics and significance of supergene karst of the upper permian changxing Formation in puguang gasfield, Sichuan basin. *J. Palaeogeogr.* 21 (6), 901–912. doi:10.7605/gdlxb.2019.06.061

Yang, W., Hu, M. Y., Song, H. J., and Hu, Z. H. (2008). Diagenesis of middle and upper cambrian reservoirs in southern part of Sichuan basin. *Mar. Orig. Pet. Geol.* 13 (4), 29–36. doi:10.3969/j.issn.1672-9854.2008.04.005

Yang, X. F., Huang, X., Wang, X. Z., Wang, Y. P., Li, K., and Zeng, D. M. (2019a). Origin of crystal dolomite and its reservoir formation mechanism in the Xixiangchi Formation, upper cambrian in southeastern Sichuan Basin. *Carbonates Evaporites* 34, 1537–1549. doi:10.1007/s13146-019-00499-y

Zenger, D. H., Dunham, J. B., and Ethington, R. L. (1980). Concepts and moels of dolomitization. *Spec. Publ. -SEPM* 28, 1–320. doi:10.2110/pec.80.28

Zhai, G. M., Wang, S. H., and He, W. Y. (2012). Hotspot trend and enlightenment of global ten-year hydrocarbon exploration. *Acta Pet. Sin.* 33 (S1), 14–19.

Zhang, J., Shou, J. F., Zhang, T. F., Pan, L. Y., and Zhou, J. G. (2014b). New approach on the study of dolomite origin:the crystal structure analysis of dolomite. *Acta Sedimentol. Sin.* 32 (3), 550–559.

Zhang, J. Y., Ni, X. F., Wu, X. N., Li, W. Z., Hao, Y., Chen, Y. N., et al. (2017). Main controlling factors and distribution of high quality reservoirs of deep buried

dolomite in typical craton in China. *Nat. Gas. Geosci.* 28 (8), 1165–1175. doi:10.1016/j.jnggs.2018.04.003

Zhang, M. L., Xie, Z. Y., Li, X. Z., Gu, J. R., Yang, W., and Liu, M. Z. (2010). Characteristics of lithofacies paleogeography of cambrian in Sichuan basin. *Acta Sedimentol. Sin.* 28 (1), 128–139.

Zhang, X. F., Liu, B., Cai, Z. X., and Hu, W. X. (2010a). Dolomitization and carbonate reservoirs formation. *Geol. Sci. Technol. Inf.* 29 (3), 79–85. doi:10.3969/j.issn.1000-7849.2010.03.012

Zhao, W. Z., Shen, A. J., Hu, S. Y., Pan, W. Q., and Qiao, Z. F. (2012). Types and distributional features of Cambrian-Ordovician dolostone reservoirs in Tarim Basin, northwestern China. *Acta Petrol. Sin.* 28 (3), 758–768.

Zhao, Y. Y., and Zheng, Y. F. (2011). Diagenesis of carbonate sediments. *Acta Petrol. Sin.* 27 (2), 501–519.

Zhou, L., Kang, Z. H., Liu, Z., Kong, J. X., and Chen, Y. (2014). Characteristics of Xixiangchi group carbonate reservoirs space in leshan-longnvsi palaeouplift, Sichuan basin. *J. Central South University:Science Technol.* 45 (12), 4393–4402.

Zhou, Z., Wang, X. Z., Yin, G., Yuan, S. S., and Zeng, S. J. (2016). Characteristics and Genesis of the (sinian) dengying formation reservoir in central sichuan, China. *J. Nat. Gas Sci. Eng.* 29, 311–321. doi:10.1016/j.jngse.2015.12.005

Zhu, D. Y., Jin, Z. Y., Hu, W. X., and Zhang, X. F. (2008). Effects of deep fluid on carbonates reservoirs in Tarim Basin. *Geol. Rev.* 54 (3), 348–357. doi:10.3321/j.issn:0371-5736.2008.03.008

Zhu, D. Y., Meng, Q. Q., Jin, Z. J., Liu, Q. Y., and Hu, W. X. (2015). Formation mechanism of deep Cambrian dolomite reservoirs in the Tarim basin, northwestern China. *Mar. Petroleum Geol.* 59, 232–244. doi:10.1016/j.marpetgeo.2014.08.022

Zhu, Y. G., Zhang, S. C., Liang, Y. B., Ma, Y. S., Zhou, G. Y., and Dai, J. X. (2006). Characteristics of gas reservoirs with high content of H_2S in the Northeastern Sichuan Basin and the consumption of hydrocarbons due to TSR. *Acta Sedimentol. Sin.* 24 (2), 300–308. doi:10.3969/j.issn.1000-0550.2006.02.020

Zou, C. N., Du, J. H., Xu, C. C., Wang, Z. C., Zhang, B. M., Wei, G. Q., et al. (2014). Formation, distribution, resource potential and discovery of the Sinian-Cambrian giant gas field, Sichuan Basin, SW China. *Petroleum Explor. Dev.* 41 (3), 278–293. doi:10.1016/S1876-3804(14)60036-7